

Deep Tabular Representation Corrector

Hangting Ye, Peng Wang, Wei Fan, Xiaozhuang Song, He Zhao, *Member, IEEE*, Dandan Guo*, Yi Chang*,
Senior Member, IEEE

Abstract—Tabular data have been playing a mostly important role in diverse real-world fields, such as healthcare, engineering, finance, etc. The recent success of deep learning has fostered many deep networks (e.g., Transformer, ResNet) based tabular learning methods. Generally, existing deep tabular machine learning methods are along with the two paradigms, i.e., in-learning and pre-learning. In-learning methods need to train networks from scratch or impose extra constraints to regulate the representations which nonetheless train multiple tasks simultaneously and make learning more difficult, while pre-learning methods design several pretext tasks for pre-training and then conduct task-specific fine-tuning, which however need much extra training effort with prior knowledge. In this paper, we introduce a novel deep Tabular Representation Corrector, TRC, to enhance any trained deep tabular model’s representations without altering its parameters in a model-agnostic manner. Specifically, targeting the representation shift and representation redundancy that hinder prediction, we propose two tasks, i.e., (i) *Tabular Representation Re-estimation*, that involves training a shift estimator to calculate the inherent shift of tabular representations to subsequently mitigate it, thereby re-estimating the representations and (ii) *Tabular Space Mapping*, that transforms the above re-estimated representations into a light-embedding vector space via a coordinate estimator while preserves crucial predictive information to minimize redundancy. The two tasks jointly enhance the representations of deep tabular models without touching on the original models thus enjoying high efficiency. Finally, we conduct extensive experiments on state-of-the-art deep tabular machine learning models coupled with TRC on various tabular benchmarks which have shown consistent superiority.

Index Terms—Tabular data, deep neural networks, tabular representation learning.

I. INTRODUCTION

TABULAR data, typically represented as tables with rows standing for the data samples and columns standing for the heterogeneous feature variables (e.g. categorical and numerical features), is a fundamental data type across diverse fields, including healthcare [1], finance [2], engineering [3] and psychology [4]. Unlike perceptual data (e.g., image and text), tabular data lacks prior structural information [5], making it essential to discover relationships within the data without relying on preconceived structures. Over the course of several

decades, tabular machine learning has garnered significant attention from researchers, transitioning from traditional machine learning techniques (e.g. linear regression [6], logistic regression [7]) to more advanced tree-based approaches (e.g. XGBoost [8], CatBoost [9]). Recently, witnessing the great success of deep learning in many domains such as computer vision [10], [11] and natural language processing [12], researchers have observed there is still a large gap in the effective usage of deep learning methods in the tabular domain [5], [13].

Research on deep tabular machine learning currently encompasses two main directions: in-learning and pre-learning styles. For the in-learning style, typically neural network backbones with different architectures are trained from scratch, or additional constraints are applied to regularize the representations. For example, AutoInt [14] transforms features to embeddings and applies a series of attention-based transformations to the embeddings based on Transformer [15]. FT-Transformer [13] further improves AutoInt through better token embeddings. SNN [16] proposes an MLP-like model with neuron activations aiming for zero mean and unit variance, fostering an effective regularization for learning complex representations. Kadra *et al.* [17] further regularizes the MLP with multiple modern regularization techniques. Recently, PTaRL [18] constructs a new projection space and projects data samples into this space, facilitating the learning of disentangled representations with constraints tailored for tabular data. However, these techniques are limited to learning from scratch, or training multiple loss functions simultaneously, leading to difficulties in effectively optimizing the target loss function.

Another novel line of works explore the direction of pre-learning for the tabular domain. This line of works design a set of pretext tasks that are challenging but highly relevant to the objective tasks and optimize the parameters of the backbone models via pre-training on these pretext tasks. For example, TabNet [19] and VIME [20] try to recover the corrupted inputs with auto-encoding loss. SCARF [21] utilizes a contrastive loss similar to SimCLR [22] between the sample and its corrupted counterpart. SubTab [23] incorporates a combination of both. However, these pretext tasks are often inspired by some prior knowledge and need much extra training effort.

Our paper introduces a novel deep Tabular Representation Corrector, TRC, to enhance the representations of any trained deep tabular backbone model without altering its parameters. Unlike existing approaches that directly intervene in the learning process of backbones (in-learning) or rely on prior knowledge to design pretext tasks for pre-training (pre-learning), TRC provides a cost-effective, parameter-efficient technique to enhance representations for deep tabular models to improve performance in a model-agnostic way. Besides, with TRC, we aim to solve two inherent issues hindering prediction: (i)

Hangting Ye, Peng Wang, Dandan Guo, and Yi Chang are with the School of Artificial Intelligence, Jilin University, China. Yi Chang is also with the Engineering Research Center of Knowledge-Driven Human-Machine Intelligence, Ministry of Education, China and the International Center of Future Science, Jilin University, China. E-mail: yeht22@mails.jlu.edu.cn, pwang23@mails.jlu.edu.cn, guodandan@jlu.edu.cn, yichang@jlu.edu.cn.

Wei Fan is with the School of Computer Science, University of Auckland, New Zealand. E-mail: wei.fan@auckland.ac.nz.

Xiaozhuang Song is with the Chinese University of Hong Kong, Shenzhen, China. E-mail: xiaozhuangsong1@link.cuhk.edu.cn.

He Zhao is with CSIRO’s Data61 and Monash University, Australia. E-mail: he.zhao@data61.csiro.au.

*Dandan Guo and Yi Chang are the corresponding authors.

Our code is available at <https://github.com/HangtingYe/TRC>.

Representation Shift, where inherent noise within the observations can lead the learned representations by deep tabular models to deviate from the ideal optimal representations, and (ii) *Representation Redundancy*, where deep tabular models may incorporate redundant information in the representation space, thereby resulting in inaccurate prediction.

To overcome the aforementioned challenges, we propose two tasks: *Tabular Representation Re-estimation* and *Tabular Space Mapping*. Specifically, for *Tabular Representation Re-estimation*, we fit an estimator to compute and eliminate the latent shift within each representation of the trained tabular model, thereby re-estimating the representations. For *Tabular Space Mapping*, we transform the re-estimated representations into a newly defined space characterized by a set of embedding vectors to condense the information. Furthermore, additional strategies are proposed to preserve the critical knowledge for prediction. The redundant information is removed by reducing the information capacity while preserving critical information necessary for accurate prediction. The contributions of this paper include:

- We propose a novel tabular representation corrector, TRC, for deep tabular machine learning, which enhances the learned representations of any trained deep tabular backbone without altering its parameters in a model-agnostic manner.
- We propose two tasks in TRC, i.e., *Tabular Representation Re-estimation* and *Tabular Space Mapping* to overcome the issues of Representation Shift and Representation Redundancy respectively hindering tabular predictions.
- We conduct extensive experiments on state-of-the-art (SOTA) deep tabular models coupled with TRC on various tabular benchmarks. The comprehensive results along with analysis and visualizations demonstrate the effectiveness of TRC, even in challenging scenarios involving missing values and reduced training samples.

II. RELATED WORK

Inspired by the success of deep learning in CV [10] and NLP [12], numerous deep learning methods have been proposed for tabular domain to accomplish prediction tasks. Research on deep tabular machine learning currently encompasses two main directions: in-learning and pre-learning styles.

A. In-learning for Tabular Data

In the context of the *in-learning* style, neural networks with various architectures are typically trained from scratch, or extra constraints are applied to better regulate learned representations [14], [13], [24], [16], [17], [25], [18]. Among these approaches, AutoInt [14] transforms input features into embeddings, which are then processed through a series of attention-based transformations. Building on this, FT-Transformer [13] improves upon AutoInt by enhancing token embeddings, using element-wise multiplication for numerical features and element-wise lookup tables for categorical features. Similarly, ResNet for tabular data [13] demonstrates significant performance improvements. DCN2 [24] introduces a feature-crossing module that combines linear layers and multiplication operations with an MLP-like structure, enhancing its ability

to capture feature interactions. SNN [16] proposes neuron activations designed to maintain zero mean and unit variance, promoting better regularization. *Kadra et al.* [17] further regularizes the MLP by searching for the optimal combination of multiple regularization techniques for each dataset using a joint optimization over the decision on which regularizers to apply. TANGOS [25] proposes a new regularization technique for tabular data, encouraging neurons to focus on sparse, non-overlapping input features. More recently, PTaRL [18] constructs a new projection space consisting of prototypes and projects data samples into this space, facilitating the learning of disentangled representations with constraints tailored for tabular data. However, these techniques are limited to learning from scratch, or training multiple loss functions simultaneously, leading to difficulties in effectively optimizing the target loss function.

B. Pre-learning for Tabular Data

Pre-learning methods design several pretext tasks for pre-training and then conduct task-specific fine-tuning [20], [21], [23], [26], [27]. For instance, VIME [20] introduces a novel pretext task that estimates mask vectors from corrupted tabular data alongside a reconstruction task for self-supervised learning. SCARF [21] employs a contrastive loss akin to SimCLR [22], contrasting samples with their corrupted versions by corrupting a random subset of features. SubTab [23] divides the input features to multiple subsets, and then incorporates a combination of both reconstruction and contrastive loss. SAINT [26] enhances this by integrating a Transformer with row-wise attention to capture inter-sample interactions and contrastive information during pre-training. In addition, *Rubachev et al.* [27] indicates that pre-training MLP with several self-supervised learning objectives could achieve promising results. However, these pretext tasks are often inspired by some prior knowledge and need much extra training effort. Recently, alternative approaches have leveraged external information outside target dataset during pre-training to enhance deep learning for tabular data. TransTab [28] incorporates feature name information into Transformer to achieve cross table learning. XTab [29] pre-trains Transformer on a variety of datasets and aims to enhance tabular deep learning on a previously unseen dataset. These methods need additional information outside target dataset and also increase the time complexity, which we do not consider as closely related baseline methods to ours as the primary goal, motivation, and methodology are different.

Different from existing approaches that directly intervene in the learning process of deep tabular models (*in-learning*), or rely on prior knowledge or additional information outside the target dataset to design pretext tasks for pre-training thus increasing time overhead (*pre-learning*), tabular representation corrector provides a cost-effective, parameter-efficient technique to enhance representations for deep tabular models.

III. PROBLEM FORMULATIONS

Notation. Denote the i -th sample as (x_i, y_i) , where $x_i = (x_i^{(num)}, x_i^{(cat)}) \in \mathbb{X}$ represents numerical and categorical

features respectively and $y_i \in \mathbb{Y}$ is the corresponding label. A real-world tabular dataset $\mathcal{D} = \{(x_i, y_i)\}_{i=1}^N$ is a collection of N data samples. We denote the training set as \mathcal{D}_{train} , the validation set for early stopping as \mathcal{D}_{val} , and the test set for the final evaluation as \mathcal{D}_{test} . We consider deep learning for supervised tabular prediction tasks: regression $\mathbb{Y} = \mathbb{R}$, binary classification $\mathbb{Y} = \{0, 1\}$ and multiclass classification $\mathbb{Y} = \{1, \dots, C\}$. The goal is to obtain an accurate deep tabular model $F(\cdot; \theta) : \mathbb{X} \rightarrow \mathbb{Y}$ trained on \mathcal{D}_{train} , that minimizes the expected loss $\mathbb{E}[\mathcal{L}(F(x; \theta), y)]$. Here, \mathcal{L} denotes a task-specific loss function, typically the mean squared error for regression and the cross-entropy loss for classification.

In-learning and Pre-learning. Recall that the deep tabular model $F(\cdot; \theta)$ usually includes the backbone $G_f(\cdot; \theta_f)$ parameterized with θ_f and prediction head $G_h(\cdot; \theta_h)$ parameterized with θ_h . Standard in-learning methods aim to minimize the following loss function:

$$\min_{\theta_f, \theta_h} \frac{1}{N} \sum_{i=1}^N \mathcal{L}(G_h(z_i; \theta_h), y_i), \quad z_i = G_f(x_i; \theta_f), \quad (1)$$

where N is the size of \mathcal{D}_{train} , z_i denotes the representation extracted by $G_f(x_i; \theta_f)$. In some cases, additional constraints may be optimized simultaneously. The trained $G_h(G_f(\cdot; \theta_f); \theta_h)$ is then used for prediction.

For pre-learning methods, pretext tasks $\mathcal{D}_s = \{(x_i^s, y_i^s)\}_{i=1}^N$, such as reconstructing original features from corrupted ones, are designed to pre-train the backbone $G_f(\cdot; \theta_f)$:

$$\min_{\theta_f, \theta_h^s} \frac{1}{N} \sum_{i=1}^N \mathcal{L}(G_h^s(z_i^s; \theta_h^s), y_i^s), \quad z_i^s = G_f(x_i^s; \theta_f), \quad (2)$$

where N is the size of \mathcal{D}_s and G_h^s is used to predict y_i^s based on z_i^s . After pre-training, the backbone $G_f(\cdot; \theta_f)$ can be used to extract better data representations. A new head $G_h(\cdot; \theta_h)$ is then attached to the trained backbone $G_f(\cdot; \theta_f)$ to predict the true labels, and either $G_h(\cdot; \theta_h)$ or both $G_h(\cdot; \theta_h)$ and $G_f(\cdot; \theta_f)$ are further optimized (as in Eq. 1).

Tabular Representation Corrector (TRC). In this paper, we consider the problem of enhancing the representation $z = G_f(x; \theta_f)$ produced by a trained deep tabular backbone, while fixing the whole parameters of $G_f(\cdot; \theta_f)$. To achieve this, TRC introduces a learnable correction module $G_p(\cdot; \theta_p)$, which takes the frozen representation z as input and outputs an improved representation $G_p(z; \theta_p)$. A new head $G_h(\cdot; \theta_h)$ is then attached to $G_p(\cdot; \theta_p)$ for label prediction. During training, only $G_p(\cdot; \theta_p)$ and $G_h(\cdot; \theta_h)$ are updated. TRC applies regardless of whether the backbone $G_f(\cdot; \theta_f)$ was trained in an in-learning or pre-learning manner.

IV. METHODOLOGY

A. Motivation

In the context of deep tabular machine learning, the inherent heterogeneity of features poses significant challenges to achieving satisfactory performance using deep models. Existing approaches learn tabular representations by directly intervening in the learning process of deep tabular models (in-learning) or designing pretext tasks for pre-training based

on prior knowledge or additional information outside the target dataset (pre-learning). We propose a novel deep Tabular Representation Corrector (TRC), that provides a cost-effective, parameter-efficient technique to enhance the representations of trained deep tabular models. Specifically, the TRC could solve two inherent representation issues hindering predictions.

(i) *Representation Shift.* As stated by [30], [5], there is a natural possibility of noise in the collection process due to the heterogeneous nature of tabular data. In this work, we claim that such inherent but unobserved noise within the original observations can lead the representations extracted by deep tabular models to deviate from the ideal optimal representations (called representation shift in this paper), thereby decreasing the model performance. To verify this point, we perturb the original features with noise as a form of data augmentation, leading to the deteriorated performance of existing deep tabular models as illustrated in Fig. 1. Moreover, to further substantiate the impact of data noise on deep tabular models, we systematically increase the noise ratio and observe a consistent decline in model performance. Therefore, given the well-trained deep tabular models learned by the original observed tabular dataset, we assume that they might be limited in extracting optimal representations due to the existence of inherent noise in tabular data.

(ii) *Representation Redundancy.* To measure the complexity of representation space, we perform singular value decomposition (SVD) on the representations $\mathcal{Z} = \{z_i\}_{i=1}^N \in \mathbb{R}^{N \times D}$ to obtain: $\mathcal{Z} = \mathbf{U}\Sigma\mathbf{V}^T$ and introduce singular value entropy (SVE) as follows:

Definition 1. Singular Value Entropy. The singular value entropy (SVE) is defined as the entropy of normalized singular values:

$$\text{SVE} = - \sum_{i=1}^D \frac{\sigma_i}{\sum_{j=1}^D \sigma_j} \log \frac{\sigma_i}{\sum_{j=1}^D \sigma_j}, \quad (3)$$

where N is the number of samples, D is the dimensionality, \mathbf{U} and \mathbf{V} denote the left and right singular vector matrices, respectively, and Σ denotes the diagonal singular value matrix $\{\sigma_i\}_{i=1}^D$. The singular value spectrum is widely considered to be related to the generalization performance [31], [32], [33]. SVE measures the flatness of the singular value distribution [34]. Greater SVE values in the latent space indicate a more comprehensive capture of data structure and a higher level of information content within the latent space. However, it is observed in Fig. 2 that existing deep tabular models with higher SVE do not necessarily yield better performance; rather, the models with better performance often exhibit relatively lower SVE. For each setting, we conduct multiple experiments with random initialization. This observation suggests that, due to feature heterogeneity, deep tabular models may incorporate redundant information in the representation space, thereby affecting accurate prediction.

Targeting the above two inherent representation issues, we propose two tasks, i.e., (i) *Tabular Representation Re-estimation*, which involves training a shift estimator to calculate and mitigate the inherent shift in the representation $z = G_f(x; \theta_f)$ extracted by a trained deep tabular backbone, thereby re-estimating z , and (ii) *Tabular Space Mapping*,

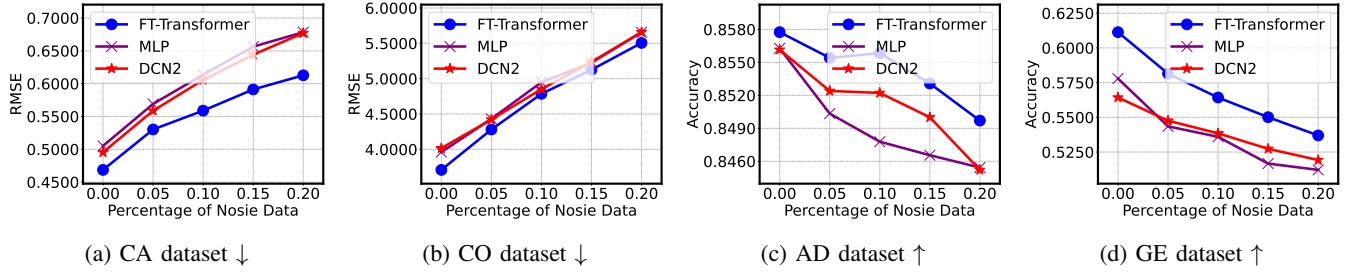


Fig. 1: The performance of deep tabular models with varying noise levels in observations. FT-Transformer, MLP, and DCN2 indicate different deep tabular models. For regression tasks, lower RMSE is better, and for classification tasks, higher accuracy is better.

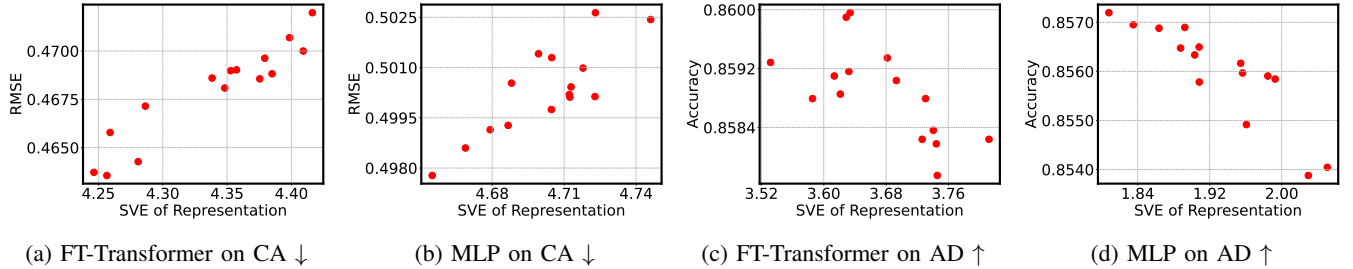


Fig. 2: The relation between model performance and the corresponding SVE values of representations. For each subfigure, we conduct experiment on multiple random seeds. We find that deep tabular models with higher SVE often yield lower performance.

which transforms the re-estimated representation into a light-embedding vector space via a coordinate estimator, aiming to preserve critical predictive information while reducing redundancy. These two tasks jointly enhance the frozen representation z without altering $G_f(\cdot; \theta_f)$ thus enjoying high efficiency. During inference, for each test sample (notably, we do not add any noise to the test dataset), the representation produced by the fixed $G_f(\cdot; \theta_f)$ is sequentially processed by the shift estimator and the coordinate estimator to obtain a calibrated representation. Note that TRC, as a general representation learning framework, is model-agnostic such that it can be coupled with any trained deep tabular backbone $G_f(\cdot; \theta_f)$ to learn better representations. In the following, we will elaborate on the details of TRC. Fig. 3 gives an overview framework.

B. Tabular Representation Re-estimation

Due to feature heterogeneity, deep tabular models are susceptible to the influence of various types of noise as depicted in Fig. 1, which often leads to undesirable shifts in the models' latent space. This causes the learned representations (sub-optimal representations) to deviate from the ideal optimal ones. Directly intervening in the learning process of deep tabular models or designing appropriate pretext tasks is challenging due to the unknown optimal representations. To alleviate this issue, we propose a task via representation re-estimation to approximate and mitigate inherent shift in the sub-optimal representations of the trained deep tabular models. This process involves the following stages: (i) Approximated Optimal Representations Searching, which identifies a subset of representations containing the least shift information towards

the ideal optimal representations; (ii) Inherent Shift Learning, where varying types of random signals are manually injected into the above selected approximated optimal representations to train a robust shift estimator capable of modeling the inherent shift present in sub-optimal representations; and (iii) Re-estimation of Sub-optimal Representations, which applies the learned shift estimator to remove the estimated shift from each sub-optimal representation, thereby re-estimating the representations.

Approximated Optimal Representations Searching. By estimating the shift information present in each sub-optimal representation, we can infer the overall shift information within the whole representations of deep tabular models. To achieve this, we propose searching a subset of samples with relatively optimal representations (approximated optimal representations) and then manually introducing shift information into these representations to simulate representations with shift, i.e. simulated sub-optimal representations. With the simulated sub-optimal representations and their corresponding shift, we can fit a shift estimator to compute the overall shift information, which would be introduced in the subsequent stage. To obtain the set of samples with approximated optimal representations, we first introduce an assumption as follows:

Assumption 1. *If we possess a deep tabular model $F(\cdot; \theta) = G_h(G_f(\cdot; \theta_f); \theta_h)$ trained on \mathcal{D}_{train} , then there exists a set of samples $\mathcal{D}_o \subseteq \mathcal{D}_{val}$ with lowest gradient norms among \mathcal{D}_{val} . $\forall (x, y) \in \mathcal{D}_o$, the following condition holds:*

$$\text{Rank}(\|\nabla_{\theta_f} \mathcal{L}(F(x; \theta), y)\|_p^q / |\mathcal{D}_{val}|) \leq \tau, \quad (4)$$

where $\text{Rank}(\cdot)$ denotes the ranking (integer) in ascending order within \mathcal{D}_{val} , $\|\cdot\|_p^q$ denotes the q square of the L_p norm,

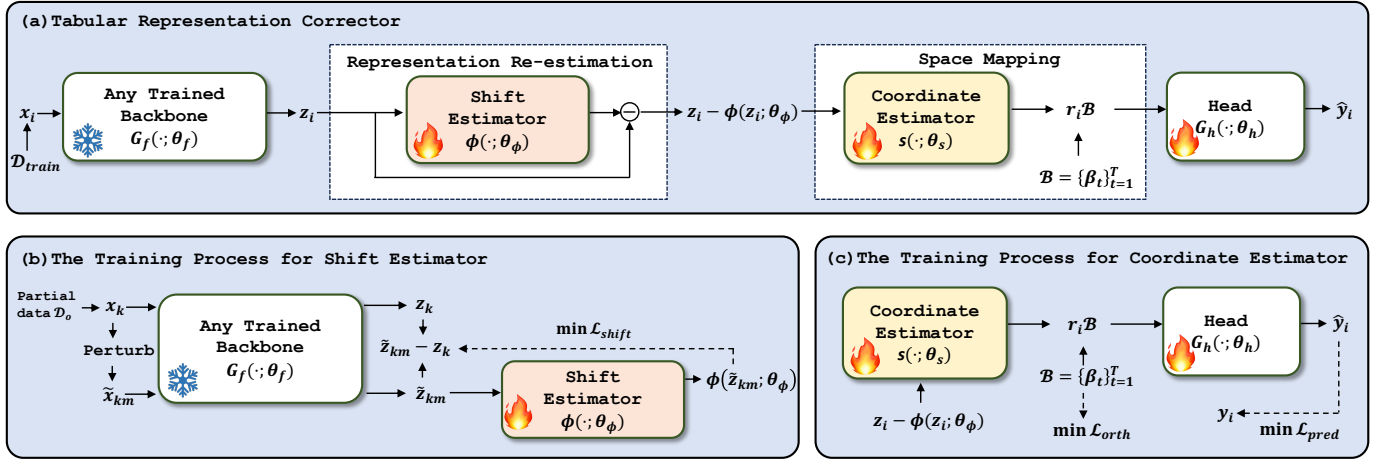


Fig. 3: The framework of Tabular Representation Corrector (TRC). Subfigure (a) illustrates the overall TRC framework, subfigure (b) presents the training process for the shift estimator of TRC, and subfigure (c) presents the training process for the coordinate estimator of TRC. Here, $z_i = G_f(x_i; \theta_f)$ is the output of any trained backbone. z_i would be enhanced via two tasks. In subfigure (b), the explicitly perturbed samples are only used for training the shift estimator. During the test stage, we feed the representations extracted by the existing trained deep tabular model, which are from the test dataset (notably, we do not add any noise to the test dataset), into the shift estimator followed by the coordinate estimator to achieve the calibrated representations of test samples.

\mathcal{L} denotes the supervised loss function, and τ denotes the threshold that defines \mathcal{D}_o .

After the trained backbone $G_f(\cdot; \theta_f)$ is obtained, we proceed to compute the gradient norms for each sample across \mathcal{D}_{val} . The searching process is conducted on \mathcal{D}_{val} to prevent overfitting and reduce the time cost. Based on Assumption 1, we assume that \mathcal{D}_o 's corresponding representation set $\mathcal{Z}_o = \{z_k = G_f(x_k; \theta_f) | (x_k, y_k) \in \mathcal{D}_o, k \in \{1, 2, \dots, K\}\}$, where K denotes the size (the threshold τ is set to 0.01 by default), contains those with the least shift information towards the ideal optimal representations, thus \mathcal{Z}_o could be treated as the approximated optimal representations.

Inherent Shift Learning. After acquiring the approximated optimal representations $\mathcal{Z}_o = \{z_k = G_f(x_k; \theta_f) | (x_k, y_k) \in \mathcal{D}_o, k \in \{1, 2, \dots, K\}\}$, we guide the training process of the shift estimator ϕ by incorporating different types of shift signals into the approximated optimal representations \mathcal{Z}_o to generate simulated sub-optimal representations $\tilde{\mathcal{Z}}_o = \{\tilde{z}_{km}\}_{k,m=1}^{K,M}$ and the corresponding shift information $\Delta = \{\Delta_{km}\}_{k,m=1}^{K,M}$, which is as follows:

$$\min_{\theta_\phi} \mathcal{L}_{shift} = \min_{\theta_\phi} \frac{1}{KM} \sum_{k,m=1}^{K,M} \|\phi(\tilde{z}_{km}; \theta_\phi) - \Delta_{km}\|_2^2, \quad (5)$$

$$\begin{aligned} \tilde{z}_{km} &= G_f(\tilde{x}_{km}; \theta_f) \\ &= G_f(\mathbf{m}_{km} \odot x_k + (1 - \mathbf{m}_{km}) \odot \epsilon_k; \theta_f), \end{aligned} \quad (6)$$

$$\Delta_{km} = \tilde{z}_{km} - z_k, \quad (7)$$

where $\mathbf{m}_{km} \in \{0, 1\}^d$ is a feature mask vector with feature number as d , $\epsilon_k \in \mathbb{R}^d$ is the noise that would be added to the corresponding observation x_k of z_k , M is the perturbing times. Given the feature heterogeneity of tabular data, we propose generating ϵ_k by sampling each feature element from the

empirical distribution of the corresponding column in \mathcal{D}_{train} , following previous works [20], [23], [35]. The shift estimator ϕ could be trained under the supervision of the simulated sub-optimal representations $\tilde{\mathcal{Z}}_o$ and their corresponding shift information Δ . In addition, during training, we also incorporate approximated optimal representations \mathcal{Z}_o and their corresponding shift (i.e., 0) as the supervision to prevent excessive shifts in the output of well-optimized representations. Since the potential shift within representations of real data samples may be diverse, the shift estimator ϕ has the challenge of inferring shift from a single type of simulated sub-optimal representations. To solve it, we suggest to diversify the types of simulated sub-optimal representations by applying M distinct perturbations to the observation x_k to simulate M different sub-optimal representations. Specifically, for x_k , we generate a feature mask vector \mathbf{m}_{km} , where each entry of the vector is set to 1 with probability η_k and to 0 otherwise. We then perturb x_k by $\mathbf{m}_{km} \odot x_k + (1 - \mathbf{m}_{km}) \odot \epsilon_k$, where $\mathbf{m}_{ki} \neq \mathbf{m}_{kj}$ if $i \neq j$. In addition, for x_k , η_k is sampled from a uniform distribution to diversify the mask vectors between different samples. By introducing such varying types of shift signals to \mathcal{Z}_o , the shift estimator ϕ has the potential to acquire information about the form of the real representation shift.

Re-estimation of Sub-optimal Representations. Given the learned shift estimator ϕ , we could remove the latent shift $\phi(z_i; \theta_\phi)$ present in sub-optimal representation $z_i = G_f(x_i; \theta_f)$ for any real data sample x_i to achieve representation re-estimation:

$$\Phi(z_i; \theta_\phi) = z_i - \phi(z_i; \theta_\phi), \quad (8)$$

where $\Phi(\cdot; \theta_\phi)$ is the re-estimation function. Through the re-estimation function, we refine the representation space of the trained backbone $G_f(\cdot; \theta_f)$ by removing the latent shift without altering any of the backbone's parameters. Despite

the shift removal achieved through this process, the problem of representation redundancy still exists. In the subsequent section, we will introduce another ingeniously designed task to address the issue of representation redundancy.

C. Tabular Space Mapping

The experimental results depicted in Fig. 2 reveal that in the realm of deep tabular machine learning models, elevated SVE does not consistently correlate with superior performance. This observation may be attributed to the presence of redundant information. To address this issue, we introduce a technique designed to map representations into a newly defined light embedding space. This space is characterized by clearer and more concise information, aiming to alleviate the influence of redundant information on prediction accuracy while preserving essential information crucial for prediction tasks. Additionally, two strategies are applied to regulate the light embedding space: (i) Space Compression, which compresses and transforms the complex knowledge from the original space into a compact space, and (ii) Critical Knowledge Preserving, which contains the key information for prediction. Since the inherent representation shift information also has the probability to spread into light embedding space, we suggest to apply this task after the previous task. First, we give the formal definition of light embedding space as follows:

Definition 2. Light Embedding Space (LE-Space). Given a collection of embedding vectors $\mathcal{B} = \{\beta_t\}_{t=1}^T \in \mathbb{R}^{T \times D}$, where T denotes the number of embeddings and β_t represents the t -th embedding vector in D -dimensional space, we define the LE-Space as the vector space spanned by the set \mathcal{B} . Formally, any representation in the LE-Space can be expressed as a weighted linear combination of the embedding vectors, given by:

$$r\mathcal{B} = \sum_{t=1}^T r^t \beta_t, \quad (9)$$

where $r = \{r^t\}_{t=1}^T \in \mathbb{R}^T$ denotes the coordinates. This formulation ensures that each representation in the LE-Space captures the essential characteristics encoded by the embedding vectors \mathcal{B} .

Space Compression. Since the trained backbone $G_f(\cdot; \theta_f)$ can inherently capture the interactions among features, and after applying the previous task, the original sub-optimal representation z_i have been re-estimated as $\Phi(z_i; \theta_\phi)$ (Eq. 8) to mitigate shift information, it is reasonable to predict r_i for each sample based on the re-estimated representation $\Phi(z_i; \theta_\phi)$. To obtain the target representation $r_i\mathcal{B}$ within LE-Space, we use a shared coordinate estimator $s(\cdot; \theta_s)$ with learnable θ_s to calculate the corresponding r_i by:

$$r_i = s(\Phi(z_i; \theta_\phi); \theta_s). \quad (10)$$

The embeddings are random initialized and learnable. By controlling the size T of the LE-Space to be significantly smaller than the dimensionality D of representation $\Phi(z_i; \theta_\phi)$, we can compress and transfer the information from the original space into the LE-Space.

Critical Knowledge Preserving. Directly mapping the representations could potentially result in a collapse of LE-Space learning, where part of the embedding vectors in the LE-Space become similar, thus diminishing the space's representational capacity. To diversify these embedding vectors, we define the orthogonality loss to encourage the cosine similarity of any pairs of embedding vectors to be close to 0:

$$\min_{\mathcal{B}} \mathcal{L}_{orth} = \min_{\mathcal{B}} \left(\frac{\|A\|_1}{\|A\|_2^2} + (\|A\|_1 - T)^2 \right), \quad (11)$$

where $A \in [0, 1]^{T \times T}$, $A_{ij} = \|\cos(\beta_i, \beta_j)\|_1$, and T is the number of embeddings. The first term $\frac{\|A\|_1}{\|A\|_2^2}$ encourages sparsity in A , meaning that each element $A_{ij} = \|\cos(\beta_i, \beta_j)\|_1$ should be close to 0 (indicating orthogonality between β_i and β_j) or 1. The second term promotes $\|A\|_1 \rightarrow T$, given that $A_{ii} = \|\cos(\beta_i, \beta_i)\|_1 = 1$ for all $i \in \{1, 2, \dots, T\}$, implying that the off-diagonal elements in the A to be close to 0. Furthermore, to maintain the key information for accurate prediction, we transfer the label information into the explicitly defined embedding vectors of LE-Space by:

$$\min_{\theta_s, \theta_\phi, \mathcal{B}, \theta_h} \mathcal{L}_{pred} = \min_{\theta_s, \theta_\phi, \mathcal{B}, \theta_h} \frac{1}{N} \sum_{i=1}^N \mathcal{L}(G_h(r_i\mathcal{B}; \theta_h), y_i), \quad (12)$$

where $r_i = s(\Phi(z_i; \theta_\phi); \theta_s)$ (Eq. 10), $G_h(\cdot; \theta_h)$ is the re-initialized projection head. In the new space, the information is compressed compared to the original space as the size T of embedding vectors is significantly smaller than the dimensionality D of representation $\Phi(z_i; \theta_\phi)$, while essential information crucial for prediction has been preserved. As a result, the new space contains less redundant information when contrasted with the original space. The detailed discussion is provided in Appendix J.

D. Framework Overview

Altogether, TRC requires learning the parameters of $\theta_\phi, \mathcal{B}, \theta_s$ and θ_h . During each training iteration, TRC first aims to minimize \mathcal{L}_{shift} to update θ_ϕ . Subsequently, TRC aims to minimize the combined objective of $\mathcal{L}_{orth} + \mathcal{L}_{pred}$ to update $\theta_\phi, \mathcal{B}, \theta_s$, and θ_h . These two optimization processes, which correspond to Tabular Representation Re-estimation and Tabular Space Mapping respectively, are iteratively alternated to refine the representations of deep tabular model without modifying the backbone's parameters θ_f in a model-agnostic manner. We provide the training process of TRC in Algorithm 1. For clarity, we also summarize the key notations used throughout the paper in Table VIII of Appendix A. This includes the symbols, their definitions, and dimensionalities where applicable.

Specifically, TRC first identifies a set of samples \mathcal{D}_o with lowest gradient norms and obtains the corresponding representations \mathcal{X}_o as the approximated optimal representations. We then manually generate the simulated sub-optimal representations $\tilde{\mathcal{Z}}_o$ and the corresponding shift information Δ based on \mathcal{X}_o . $\tilde{\mathcal{Z}}_o$ and Δ are used to supervise the training process of the shift estimator $\phi(\cdot; \theta_\phi)$ via \mathcal{L}_{shift} (Eq. 5). For a real data sample x_i , TRC removes the latent shift $\phi(z_i; \theta_\phi)$ on

Algorithm 1 TRC algorithm workflow.

Input: dataset $\mathcal{D}_{train}, \mathcal{D}_{val}$, trained $F(\cdot; \theta) = G_h(G_f(\cdot; \theta_f); \theta_h)$, shift estimator $\phi(\cdot; \theta_\phi)$, re-estimation function $\Phi(\cdot; \theta_\phi)$, coordinate estimator $s(\cdot; \theta_s)$, embedding vectors \mathcal{B} , number of batches B ;

- 1: Compute $\|\nabla_{\theta_f} \mathcal{L}(F(x; \theta), y)\|_p^q$ over \mathcal{D}_{val} and identify \mathcal{Z}_o based on **Assumption 1**;
- 2: Generate simulated sub-optimal representations $\tilde{\mathcal{Z}}_o$ and the corresponding shift information Δ ;
- 3: Re-initialize the parameters of $G_h(\cdot; \theta_h)$;
- 4: **while** $\theta_\phi, \mathcal{B}, \theta_s$ and θ_h has not converged **do**
- 5: Compute \mathcal{L}_{shift} (Eq. 5);
- 6: Update θ_ϕ by minimizing \mathcal{L}_{shift} through gradient descent;
- 7: **for** $i \leftarrow 1$ to B **do**
- 8: Sample minibatch;
- 9: Obtain representation $z = G_f(x; \theta_f)$;
- 10: Re-estimate representation by $\Phi(z; \theta_\phi)$;
- 11: Calculate r by $s(\Phi(z; \theta_\phi); \theta_s)$;
- 12: Transform the representation of $\Phi(z; \theta_\phi)$ to $r\mathcal{B}$;
- 13: Compute \mathcal{L}_{orth} (Eq. 11) and \mathcal{L}_{pred} (Eq. 12);
- 14: Update $\theta_\phi, \mathcal{B}, \theta_s$ and θ_h by minimizing $\mathcal{L}_{orth} + \mathcal{L}_{pred}$ through gradient descent.
- 15: **end for**
- 16: **end while**

Output: $\phi(\cdot; \theta_\phi), s(\cdot; \theta_s), \mathcal{B}, G_h(\cdot; \theta_h)$.

representation z_i to re-estimate it by $\Phi(z_i; \theta_\phi) = z_i - \phi(z_i; \theta_\phi)$ (Eq. 8), thereby alleviating the issue of representation shift. After that, the coordinate estimator $s(\cdot; \theta_s)$ is used to calculate the coordinate r_i (Eq. 10) to transform $\Phi(z_i; \theta_\phi)$ to $r_i\mathcal{B}$ within LE-Space to compress the information. In addition, TRC diversifies the embedding vectors \mathcal{B} via \mathcal{L}_{orth} (Eq. 11) and optimizes the \mathcal{L}_{pred} (Eq. 12) to preserve the critical knowledge for prediction. Therefore, TRC alleviates the issue of representation redundancy.

During inference, we feed the representations extracted by the existing trained deep tabular backbone, which are from the test dataset (notably, we do not add any noise to the test dataset), into the shift estimator followed by the coordinate estimator to achieve the calibrated representations of test samples. Note that TRC, as a general representation learning framework, is model-agnostic such that it can be coupled with any trained deep tabular backbone $G_f(\cdot; \theta_f)$ to learn better representations.

V. EXPERIMENT & ANALYSIS

A. Experimental Setup

Datasets. We consider a variety of tabular datasets, including regression, binary and multi-class classification. Specifically, the datasets include: Combined Cycle Power Plant (CO) [36], Diamonds (DI) [37], Qsar Fish Toxicity (QS) [38], California Housing (CA) [39], Pol (PO) [40], Superconductivity Data (SU) [41], Adult (AD) [42], Australian (AU) [43], Gesture Phase (GE) [44], Year (YE) [45] and Covertype (COV) [46]. The dataset properties are summarized in Table I.

TABLE I: Tabular data properties. ‘‘Objects’’ indicates the dataset size. RMSE denotes Root Mean Square Error for regression, Accuracy is used for binary and multiclass classification.

	CO	DI	QS	CA	PO	SU	AD	AU	GE	YE	COV
Objects	9568	53940	908	20640	15000	21263	48842	690	9873	515345	581012
Numerical	4	6	6	8	48	81	6	14	32	90	54
Categorical	0	3	0	0	0	0	8	0	0	0	0
Classes	-	-	-	-	-	-	2	2	5	-	7
Metric	RMSE	RMSE	RMSE	RMSE	RMSE	RMSE	Accuracy	Accuracy	Accuracy	RMSE	Accuracy

To handle categorical features, we adopt an integer encoding scheme, where each category within a column is uniquely mapped to an integer to index the embedding in the lookup table. We maintain consistent embedding dimensions for all categorical features. For numerical features, we apply the column-wise normalization method. In regression tasks, we also apply the normalization to the labels. To ensure fair comparisons, we adhere to identical preprocessing procedures and use the quantile transformation following [13] for each dataset. We split each dataset into training, validation, and test sets by the ratio of 6:2:2. The used datasets are collected in the public OpenML-AutoML Benchmark (<https://openml.github.io/automlbenchmark/>) and UCI datasets (<https://archive.ics.uci.edu/datasets>). Following previous studies [13], we use Root Mean Squared Error (RMSE) (lower is better) to evaluate the regression tasks, Accuracy (higher is better) to evaluate binary and multiclass classification tasks.

Baseline Deep Tabular Models. As the TRC is a model-agnostic paradigm, we include 13 mainstream deep tabular models, which include in-learning and pre-learning paradigms, to test TRC’s applicability and effectiveness to different predictors with diverse architectures. The baseline models include: MLP [47], DCN2 [24], SNN [16], ResNet [10], AutoInt [14], TANGOS [25], FT-Transformer [13], PTaRL [18], SCARF [21], SAINT [26] and VIME [20]. In addition, the authors of [27] indicate that pre-training MLP with several self-supervised learning objectives could achieve promising results. Therefore, we also include two of them as additional baseline methods. We implement all deep tabular baseline models’ hyperparameters following their original papers. The detailed descriptions about these models are as follows:

In-learning Style.

- MLP [47]. The Multilayer Perceptron (MLP) is a type of feedforward artificial neural network that consists of multiple layers of interconnected nodes, commonly used as a baseline model for supervised learning tasks in tabular domain.
- DCN2 [24]. This method consists of an MLP-like module and the feature crossing module (a combination of linear layers and multiplications).
- SNN [16]. An MLP-like architecture with the SELU activation that maintains zero mean and unit variance, enabling training deeper models.
- ResNet [10]. The key innovation is the use of residual connections, also known as skip connections or shortcut connections. These connections enable the network to effectively train deep neural networks, which was challenging before due to the vanishing gradient problem. In this paper,

TABLE II: Results of overall performance. ‘‘i’’ denotes in-learning and ‘‘p’’ denotes pre-learning for baseline models. The best results are highlighted in bold. The improvement of TRC over baselines is statistically significant at the 95% confidence level.

	CO ↓	DI ↓	QS ↓	CA ↓	PO ↓	SU ↓	AD ↑	AU ↑	GE ↑
MLP (i)	3.961	564.373	0.875	0.505	10.892	10.379	0.856	0.870	0.578
+TRC	3.899	558.330	0.825	0.502	10.593	10.326	0.858	0.891	0.580
DCN2 (i)	4.016	591.958	1.027	0.495	8.805	10.674	0.856	0.841	0.564
+TRC	3.858	574.453	0.879	0.493	8.790	10.584	0.857	0.862	0.584
SNN (i)	11.789	1530.293	1.018	0.896	18.517	25.498	0.847	0.848	0.550
+TRC	6.880	693.369	0.870	0.699	11.202	15.537	0.847	0.877	0.573
ResNet (i)	3.982	606.282	0.872	0.517	10.812	11.163	0.847	0.870	0.587
+TRC	3.919	615.736	0.845	0.508	10.205	10.720	0.849	0.877	0.597
AutoInt (i)	4.020	562.169	0.860	0.487	6.450	11.193	0.854	0.848	0.598
+TRC	3.960	557.423	0.829	0.477	5.885	10.826	0.858	0.891	0.606
TANGOS (i)	4.687	965.169	0.945	0.573	9.401	10.849	0.84	0.855	0.569
+TRC	4.478	886.904	0.914	0.538	9.271	10.520	0.839	0.882	0.590
FT-Transformer (i)	3.709	551.190	0.823	0.469	2.919	10.410	0.858	0.848	0.611
+TRC	3.648	543.653	0.780	0.462	2.728	10.223	0.862	0.884	0.624
PTaRL (i)	3.668	550.582	0.813	0.447	2.533	10.199	0.872	0.879	0.583
+TRC	3.423	543.671	0.775	0.427	2.412	9.724	0.889	0.890	0.619
SCARF (p)	3.856	579.610	0.863	0.520	8.310	10.324	0.858	0.862	0.589
+TRC	3.847	577.803	0.808	0.520	8.151	10.355	0.859	0.884	0.589
SAINT (p)	4.022	597.207	0.827	0.508	4.415	13.095	0.857	0.870	0.549
+TRC	3.903	557.951	0.818	0.491	4.335	12.443	0.858	0.884	0.595
VIME (p)	5.218	945.238	1.018	0.679	10.914	15.645	0.768	0.812	0.473
+TRC	4.371	612.454	0.950	0.645	7.489	15.028	0.846	0.884	0.479
MLP w/ SSL-Rec (p)	3.92	595.378	0.872	0.498	10.052	10.408	0.855	0.862	0.578
+TRC	3.859	581.511	0.825	0.499	9.796	10.335	0.856	0.884	0.595
MLP w/ SSL-Contrastive (p)	3.956	570.54	0.872	0.506	13.305	10.478	0.855	0.862	0.576
+TRC	3.923	562.671	0.825	0.502	12.803	10.436	0.856	0.884	0.587

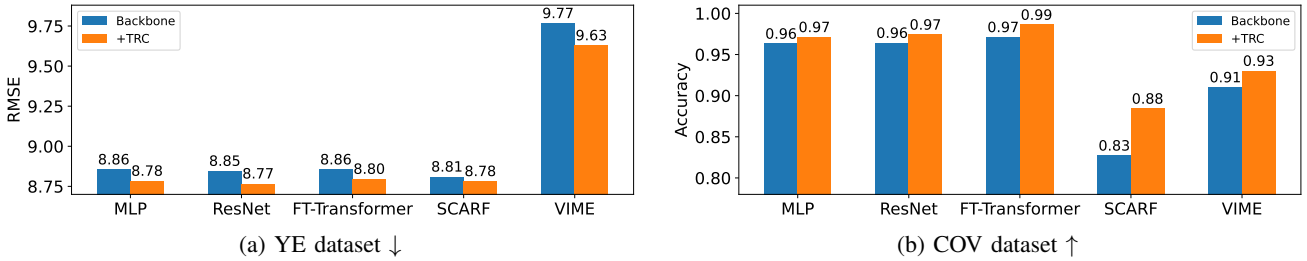


Fig. 4: Performance improvement of TRC over various backbone models on large scale datasets.

we use the ResNet for tabular data [13].

- AutoInt [14]. This method transforms features to embeddings and applies a series of attention-based transformations to the embeddings based on Transformer [15].
- TANGOS [25]. This method proposes a new regularization technique for tabular data, encouraging neurons to focus on sparse, non-overlapping input features. We adopt MLP as the base model for TANGOS.
- FT-Transformer [13]. This method is introduced by *Gorishniy et al.* [13] to further improve AutoInt through better token embeddings.
- PTaRL [18]. This method constructs a new projection space and uses Optimal Transport [48] to project data samples into this space, enabling the learning of disentangled representations with constraints designed for tabular data. We adopt FT-Transformer as the base model for PTaRL.

Pre-learning Style.

- SCARF [21]. This method extends the SimCLR framework

to tabular data by using contrastive learning.

- SAINT [26]. This method adopts attention over both rows and columns, and it includes an enhanced embedding method. Contrastive learning is used during pretraining.
- VIME [20]. This method utilizes self- and semi-supervised learning by recovering the corrupted inputs for tabular data.
- MLP w/ SSL-Rec [27]. This method aims to reconstruct the original input, given the corrupted input (the reconstruction loss is computed for all columns).
- MLP w/ SSL-Contrastive [27]. This method uses InfoNCE loss, considering corrupted inputs as positives for original inputs and the rest of the batch as negatives.

Implementation Details. Our TRC is a model-agnostic method that aims to enhance the representations of any deep tabular model $F(\cdot; \theta)$ without altering its internal architecture. To achieve it, TRC includes two tasks, i.e., Tabular Representation Re-estimation and Tabular Space Mapping. In the first task, for the q square of the L_p norm, we set $q = 1$ and

TABLE III: Analysis on the effects of different components of TRC. The best results are highlighted in bold, and the second best results are underscored.

Backbone	TR	SC	DE	CO ↓	DI ↓	QS ↓	CA ↓	PO ↓	SU ↓	AD ↑	AU ↑	GE ↑
MLP				3.961	564.373	0.875	0.505	10.892	10.379	0.856	0.87	<u>0.578</u>
	✓			3.916	563.649	0.868	0.502	10.605	<u>10.328</u>	0.858	0.87	0.571
		✓		3.92	564.141	0.845	0.505	10.631	10.349	0.858	0.862	0.568
	✓	✓		<u>3.908</u>	<u>558.52</u>	0.852	0.502	<u>10.602</u>	10.341	0.858	0.87	0.575
			✓	3.922	565.129	0.841	0.505	10.622	10.363	0.858	<u>0.877</u>	0.577
	✓	✓	✓	3.899	558.33	0.825	0.502	10.593	10.326	0.858	0.891	0.58

TABLE IV: Performance of backbone w/ TRC and deeper backbone. The depths of backbone layers are increased only for “deeper backbone”.

	CO ↓	DI ↓	QS ↓	CA ↓	PO ↓	SU ↓	AD ↑	AU ↑	GE ↑
MLP	3.961	564.373	0.875	0.505	10.892	10.379	0.856	0.870	0.578
deeper MLP	3.942	562.888	0.871	0.510	11.583	10.471	0.856	0.862	0.572
MLP+TRC	3.899	558.330	0.825	0.502	10.593	10.326	0.858	0.891	0.580
FT-Transformer	3.709	551.190	0.823	0.469	2.919	10.410	0.858	0.848	0.611
deeper FT-Transformer	3.704	559.363	0.816	0.474	2.890	10.442	0.851	0.856	0.613
FT-Transformer+TRC	3.648	543.653	0.780	0.462	2.728	10.223	0.862	0.884	0.624

$p = 1$. The threshold τ that defines the representations \mathcal{L}_o is set to 0.01. The shift estimator ϕ , which is used to calculate the potential shifts present in the representations, is a simple 2-layer fully-connected MLP. We propose generating ϵ_k by sampling each feature element from the empirical distribution of the corresponding column in \mathcal{D}_{train} , following previous works [20], [23], [35]. For mask vector \mathbf{m}_{km} , each entry of the vector is set to 1 with probability η_k and to 0 otherwise, where η_k is sampled from a uniform distribution [0.1, 0.3]. The perturbing times M for constructing the simulated sub-optimal representations is set to 3, unless otherwise specified. For the second task, the coordinate estimator s , which is used to calculate the coefficients for embedding vectors, is a simple linear layer with softmax activation function. The default number of embeddings T is set to 10, unless otherwise specified. The batch size is set to 128 and AdamW is used as the optimizer, with a learning rate of 1e-4, weight decay of 1e-5. A patience of 10 is kept for early stopping. We implement all deep tabular backbone models’ hyperparameters following their original papers. All experiments were conducted on the Ubuntu 20.04.4 LTS operating system, Intel(R) Xeon(R) Gold 5220 CPU @ 2.20GHz with single NVIDIA A40 48GB GPU and 512GB of RAM. The framework is implemented with Python 3.11.5 and PyTorch 2.0.2. To reduce the effect of randomness, the reported performance is averaged over 10 independent runs.

B. Main Results

Overall Performance. Table II has shown the performance comparison of 13 different backbones and their TRC-enhanced versions over 9 real-world tabular datasets. From the table, we can observe that TRC achieves consistent improvements over the baseline deep models in all settings, including both regression and classification scenarios. On average, TRC achieves a relative performance improvement of approximately 5.1% across all scenarios. Specifically, for regression, TRC realizes a relative performance improvement

of about 6.5% across all datasets, while for classification, TRC achieves a relative performance improvement of approximately 2.4% across all datasets. Even in cases where TRC does not outperform the baseline, its performance remains comparable. Additionally, TRC is able to enhance performance even over the best-performing baseline model for each dataset. Moreover, we conduct Wilcoxon signed-rank test (with $\alpha = 0.05$) [49] to measure the improvement significance. The results show that in all settings, the improvement of TRC over deep tabular models is statistically significant at the 95% confidence level (with p-value = $6.07e - 9$). This demonstrates the superior adaptability and generalization ability of TRC to different models and tasks. We further include experiments to verify the scalability of TRC on large scale tabular datasets, as illustrated in Fig. 4. The results show that TRC could still enhance the performance of backbone models on the large scale datasets.

Ablation Study and Comparison with Deeper Backbone Models. We further conduct ablation study to demonstrate the effectiveness of key components of TRC. Specifically, we denote the task of tabular representation re-estimation as “TR”, and for the task of tabular space mapping, we denote the process of space compression as “SC” and the strategy for diversifying the embedding vectors as “DE”. Given that the strategy for diversifying the embedding vectors should be applied after the process of space compression, we conduct a comparative analysis between the backbone integrated with TRC and its five variants. The results presented in Table III underscore that the joint effects of all of these components are crucial to achieve consistently good performance, thereby underscoring the effectiveness of TRC. More results are detailed in Appendix B. Besides, TRC is appended to the output of the backbone $G_f(\cdot; \theta_f)$ while keeping the parameters fixed. We compare the performance of the backbone coupled with TRC against backbone with deeper layers (additional 3 layers). As shown in Table IV, increasing the number of layers in backbone model does not necessarily lead to improved performance; in some cases, it even results in performance

TABLE V: Performance comparison between various fine-tuning paradigms and TRC. “i” denotes in-learning and “p” denotes pre-learning for baseline models.

	CO ↓	DI ↓	QS ↓	AU ↑
MLP (i)	3.961	564.373	0.875	0.870
+Linear Head	3.952	563.945	0.870	0.870
+Linear Head & Backbone	3.937	563.304	0.880	0.862
+MLP Head	3.950	562.076	0.862	0.870
+MLP Head & Backbone	3.934	562.427	0.857	0.870
+LoRA	3.941	563.314	0.875	0.870
+TRC	3.899	558.330	0.825	0.891
DCN2 (i)	4.016	591.958	1.027	0.841
+Linear Head	4.173	589.030	0.958	0.843
+Linear Head & Backbone	4.009	592.881	1.029	0.845
+MLP Head	4.077	586.749	0.906	0.847
+MLP Head & Backbone	4.088	591.743	0.910	0.842
+LoRA	4.001	591.903	1.021	0.849
+TRC	3.858	574.453	0.879	0.862
FT-Transformer (i)	3.709	551.190	0.823	0.848
+Linear Head	3.695	552.416	0.828	0.828
+Linear Head & Backbone	3.710	554.259	0.816	0.870
+MLP Head	3.698	549.648	0.816	0.832
+MLP Head & Backbone	3.706	556.086	0.802	0.870
+LoRA	3.683	550.241	0.823	0.862
+TRC	3.648	543.653	0.780	0.884
SCARF (p)	3.856	579.610	0.863	0.862
+Linear Head	3.870	578.389	0.842	0.867
+Linear Head & Backbone	3.871	579.757	0.856	0.870
+MLP Head	3.864	578.565	0.850	0.862
+MLP Head & Backbone	3.872	604.720	0.851	0.862
+LoRA	3.874	589.828	0.863	0.870
+TRC	3.847	577.803	0.808	0.884

degradation. Furthermore, the comparison between deeper backbone and backbone augmented with TRC highlights that the well-designed tasks can significantly enhance model representations, which is not simply achieved by increasing model depth. More results are provided in Appendix C.

Comparison with Fine-tuning Paradigm. We also compare TRC with some fine-tuning methods. Specifically, given any trained backbone models, we compare TRC against five different fine-tuning strategies in Table V: i) Linear Head: we simply attach a new linear head to a trained backbone and train only this new head; ii) Linear Head & Backbone: we use the same architecture as strategy i, but we train both new head and the whole backbone; iii) MLP Head: we replace the linear head of strategy i with a two-layer MLP as the new head, and also train this new head only; iv) MLP Head & Full Backbone: we use the same architecture as strategy iii, but we train both new head and the whole backbone; v) LoRA (Low-Rank Adaptation): we use the parameter-efficient fine-tuning strategy LoRA (Low-Rank Adaptation), that injects trainable low-rank matrices into the whole frozen backbone parameters to adapt models with minimal additional parameters. In practice, we inject low-rank matrices into all linear layers of the backbone and freeze the original weights. For all strategies, we set the learning rate to $1e-4$, which matches the learning rate used for TRC. The results show that none of these fine-tuning strategies including LoRA achieve performance comparable to TRC. The possible reason is that only training the new head or fine-tuning the backbone with conventional supervised

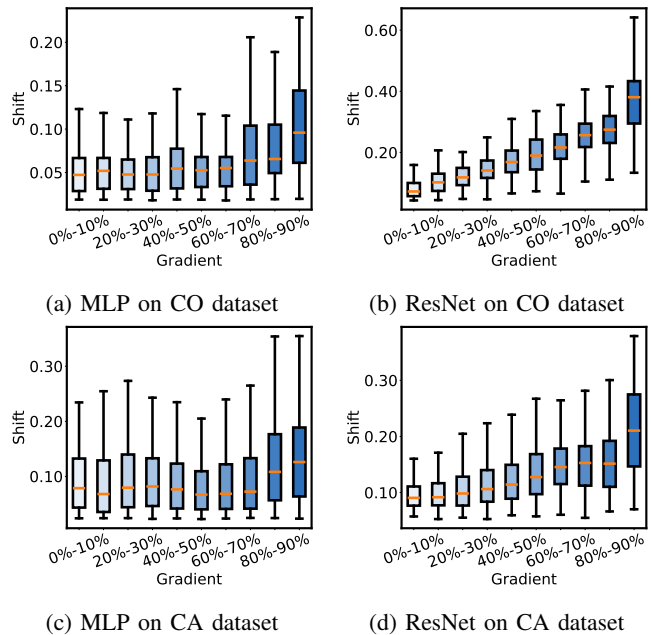


Fig. 5: Comparison of the L_1 norm of the shift information estimated by TRC on data samples with different gradients. For each data sample, the gradient is computed by $\|\nabla_{\theta_f} \mathcal{L}(x, y; \theta)\|_1$, where θ is the parameters of the trained deep tabular model. We partition the L_1 norm of gradients into 10 equally spaced intervals from low to high and count the number of samples in each interval.

training loss (already used by the trained backbone) can not provide additional useful information for representation. Different from fine-tuning methods, TRC is a representation correction method that tailor-designed for solving the inherent deep tabular backbone representations issues in a post-hoc and model-agnostic way, without altering backbone parameters. Specifically, we build a shift estimator to calculate the inherent shift of tabular representations and design a space mapping method to alleviate the influence of redundant information. To end this, we further design two unsupervised losses (please refer to Eq. 5 and Eq. 11).

C. Further Analysis

TRC enables the learning of the inherent shift by representation re-estimation. Fig. 5 illustrates the estimated shift information within the representations of trained deep tabular backbones. For the representations of the backbone $G_f(\cdot; \theta_f)$, those with larger gradients are associated with greater shift information learned by TRC. Through the task of *tabular representation re-estimation*, the shift information contained in sub-optimal representations can be gradually eliminated.

TRC reduces the redundant information by space mapping. Subfigure (a) of Fig. 6 shows the representation SVE of deep tabular backbone $G_f(\cdot; \theta_f)$ w/ and w/o TRC, and subfigure (b) shows the corresponding performance. Similar to subfigures (c) and (d). We could find that with TRC, the SVE value of the representations decreased, and the performance improved. This demonstrates that TRC reduces the redundant

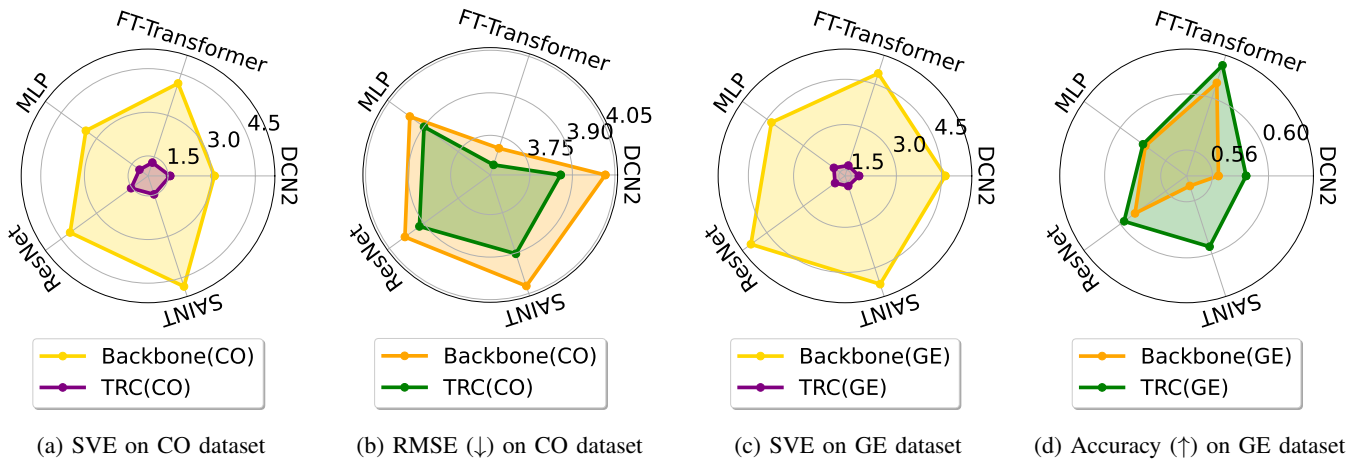


Fig. 6: SVE and performance changes of backbone models w/ and w/o TRC on different datasets. Subfigures (a) and (c) show the Singular Value Entropy (SVE) (Eq. 3) of representation space w/ and w/o TRC on different datasets. Subfigures (b) and (d) show the corresponding performance.

TABLE VI: The influence of using a small portion (1%) of validation set for training. “Train” indicates only training data are used for training model, “Val” indicates additional small portion of validation data are used for training.

	CO ↓		DI ↓		AU ↑	
	Train	Val	Train	Val	Train	Val
MLP	3.961	3.968	564.373	565.616	0.870	0.870
+TRC	3.902	3.899	559.020	558.330	0.891	0.891
FT-Transformer	3.709	3.726	551.190	550.228	0.848	0.848
+TRC	3.647	3.648	544.570	543.653	0.877	0.884

information via *tabular space mapping* to enhance the model performance.

The performance improvement comes from the effectiveness of the TRC, rather than from additional training data. Only a small portion (1%) of the validation data is used to train our shift estimator, and these additional data are not used in the remaining learning or test process. We provide additional experiment results in Table VI to show whether the improvements come from additional training data or the proposed modifications. Here, we consider two settings. One setting is that we use a portion of the training data rather than the additional validation data to train the shift estimator, making it fair when being compared with existing baselines. Another setting is that we also add a small portion (1%) of the validation data into the training set when training baseline models. As listed in Table VI, ours still outperforms the corresponding baseline even without using additional validation data. In addition, the baseline shows similar performance whether or not additional data is used, and TRC similarly demonstrates consistent performance regardless of the use of additional data. Therefore, we demonstrate that the performance improvement comes from the effectiveness of the TRC, rather than from additional training data.

The performance of TRC under missing values and reduced training data. We systematically increase the pro-

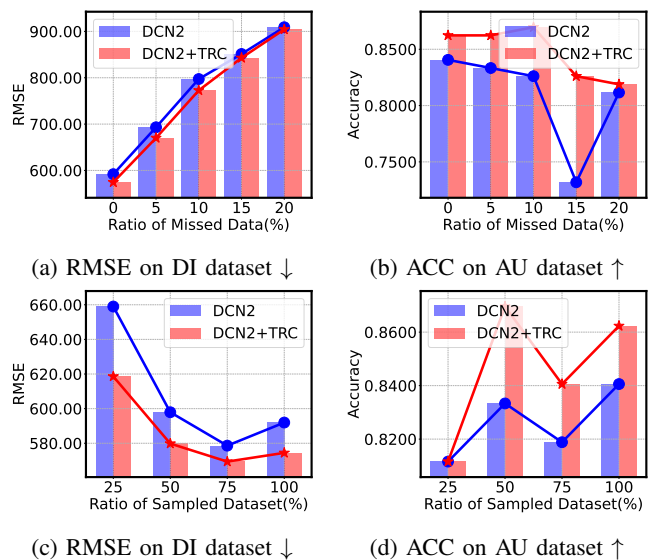


Fig. 7: The results of TRC training with missing values and fewer samples. The left two subfigures indicate the scenarios with missing values, while the right two indicate the scenarios where the number of training samples is reduced.

portion of missing values in features and reduce the proportion of training samples separately. The results in Fig. 7 indicate that as the dataset’s missing values escalate or the training sample size diminishes, the difficulty of model training intensifies, which is reflected in a decline in model performance. Nevertheless, by leveraging TRC, we are able to consistently enhance the capabilities of the deep tabular model, thereby alleviating the negative impact of data incompleteness and scarcity. More results can be found in the Appendix D.

Visualization. The TSNE visualization of learned representations in Fig. 8 demonstrates that TRC could well calibrate representations. Even only with Tabular Representation Re-estimation, the representations are more organized compared to the baseline and fine-tuning approaches, as shown in sub-

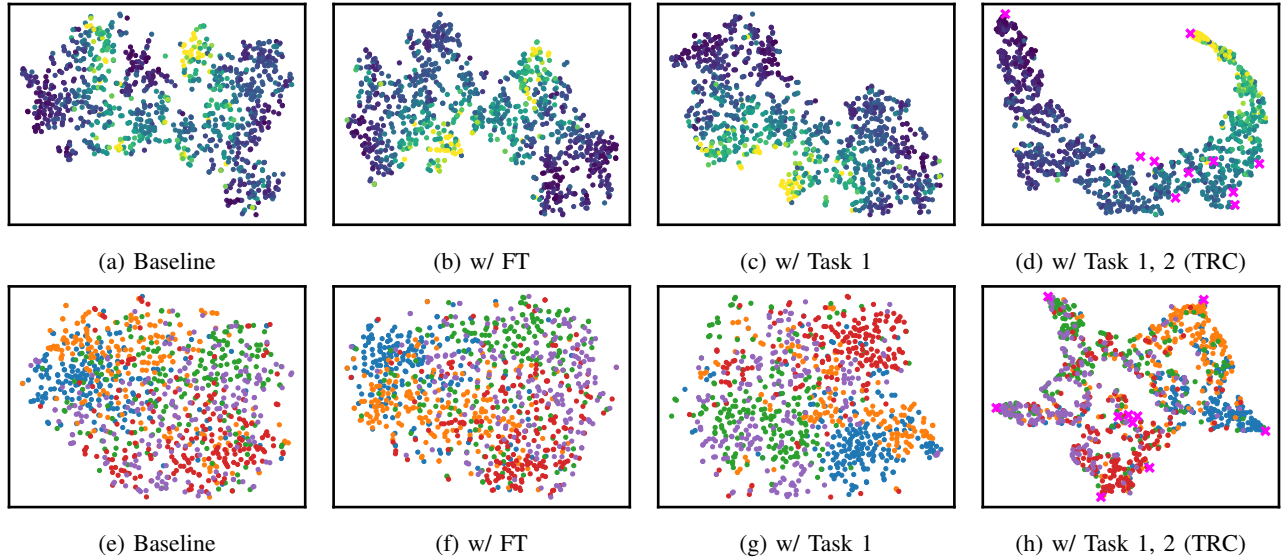


Fig. 8: The TSNE visualization of learned representations of deep tabular model, deep tabular model w/ FT (fine-tuning), deep tabular model w/ Task 1 (Tabular Representation Re-estimation) and deep tabular model w/ Task 1, 2 (Tabular Representation Re-estimation and Tabular Space Mapping) (i.e., TRC). Here, the backbone model is ResNet. The first row represents the CA dataset (regression), while the second row represents the GE dataset (classification). Different colors indicate different labels. Marker="x" indicates embedding vectors.

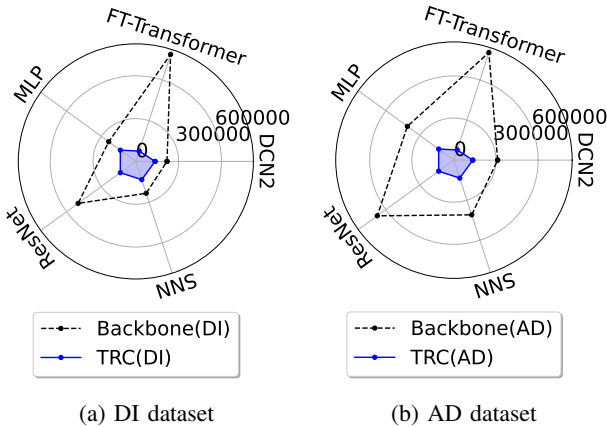


Fig. 9: The comparison of parameters between TRC and different deep tabular models. The parameters for TRC do not include the parameters for backbone models.

figure (c). We also visualize the learned embedding vectors in subfigures (d) and (h). The embedding vectors are learnable, and we encourage the embedding vectors to be orthogonal through an orthogonality loss (Eq. 11), as orthogonality is known to be helpful in improving discriminative ability [50], [51]. Our findings reveal that these embedding vectors are extensively distributed across the latent space, contributing to the effective modeling of representations. In the regression tasks, which involve continuous labels and necessitate fine-grained information for discriminative representations, the application of TRC leads to a marked improvement in the ability to differentiate between various continuous labels. Consequently, the arrangement of these representations becomes

more structured and organized. In the classification tasks, after applying TRC, representations are separated into several non-overlapping regions, where representations with similar labels are clustered together, demonstrating the method’s efficacy in enhancing the separability of the data points.

Parameters analysis and Computational efficiency. The proposed TRC provides a parameter-efficient, cost-effective technique to enhance the representations of deep tabular backbones without altering any of their parameters. As illustrated in Fig. 9, the parameter quantity of TRC is significantly lower compared to deep tabular models, particularly for the FT-Transformer model, which inherently has a large number of parameters. More results are provided in Appendix E. In addition, since TRC does not need to retrain the deep tabular backbone, the training time of TRC is noticeably reduced compared to the deep tabular model in most cases. The inference cost of TRC is also much smaller compared to deep tabular backbones, thus will not introduce high inference overhead to the existing backbones. Details of training and inference time cost are provided in Table XI and Table XII in Appendix F.

The Threshold of Selected Approximated Optimal Representations τ . To verify the robustness of TRC to violations of proposed assumption and the choice of the threshold τ , we compare TRC against two variants: (i) TRC (Random) that randomly selects samples and (ii) TRC (Highest) that selects samples with the highest gradient norms. We provide these comparisons across a wide range of threshold τ in Fig. 10. Here, the backbone model is DCN2. Additional results are provided in Fig. 21 in Appendix I. The results show that TRC benefits from selecting samples with the lowest gradient norms, as hypothesized. When the assumption is violated, e.g., by selecting random samples or those with the highest

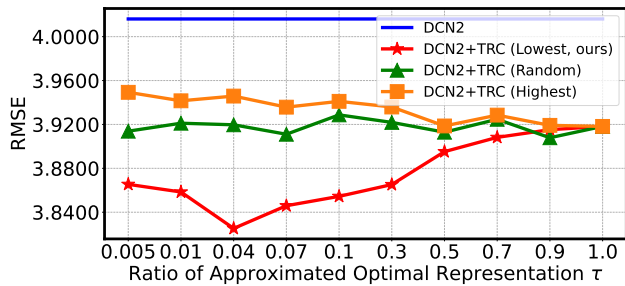


Fig. 10: Comparison with different approximated optimal representation selection strategies across a wide range of threshold τ on CO dataset \downarrow .

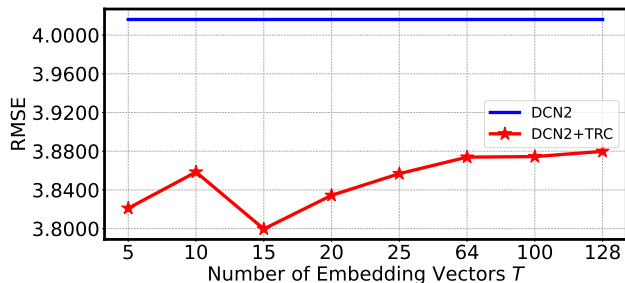


Fig. 11: The performance of TRC with varying number of embedding vectors on CO dataset \downarrow .

gradient norms, TRC still improves the performance of the backbone model, albeit to a lesser extent. When the threshold τ is relatively low (e.g., less than 0.3), the performance of TRC is stable. As τ increases further, samples with high gradient norms are also selected and the corresponding performance degrades slightly, but TRC could still enhance the performance of backbone model. Overall, TRC is robust to the proposed assumption and choice of the threshold τ . We suggest to select the samples with the lowest gradient norms using a conservative threshold (less than 0.3), which balances performance gain and computational cost.

Additional Experiments. A representative case of the sensitivity analysis on the number of embedding vectors is provided in Fig. 11. Additional results are presented in Fig.22 of Appendix I, and a more in-depth discussion is provided in Appendix J. Additional sensitivity analysis w.r.t. the weight of loss function \mathcal{L}_{orth} , and the perturbing times for constructing simulated sub-optimal representations in Inherent Shift Learning in Appendix I. The comparison between TRC and tree-based methods is detailed in Table VII. We also provide the visualizations of learned coefficients r (Eq. 10) for embedding vectors in Appendix G. The discussion about how well the computed shift by shift estimator can model the real inherent shift is provided in Appendix K, and the limitation discussion about **Assumption 1** is presented in Appendix L.

VI. CONCLUSION

In this paper, we introduce a novel deep Tabular Representation Corrector, TRC, to enhance trained tabular models through two specific tasks without altering their parameters

TABLE VII: Comparison with tree-based methods.

	DI \downarrow	QS \downarrow	PO \downarrow	AU \uparrow
FT-Transformer+TRC	543.653	0.780	2.728	0.884
CatBoost [9]	546.827	0.817	4.641	0.855
XGBoost [8]	559.680	0.820	4.936	0.862

in a model-agnostic way. Specifically, TRC could solve two inherent representation issues, i.e., *representation shift* and *representation redundancy*. We propose two tasks, i.e., (i) *Tabular Representation Re-estimation*, that involves training a shift estimator to calculate the inherent shift of tabular representations to subsequently mitigate it, thereby re-estimating the representations, and (ii) *Tabular Space Mapping*, that transforms the re-estimated representations into a light-embedding vector space while preserves crucial predictive information to minimize redundancy. The empirical results on various real world tasks demonstrated the effectiveness of TRC for tabular deep learning. Our work can shed some light on developing better algorithms for similar tasks.

REFERENCES

- [1] M. Hernandez, G. Epelde, A. Alberdi, R. Cilla, and D. Rankin, “Synthetic data generation for tabular health records: A systematic review,” *Neurocomputing*, vol. 493, pp. 28–45, 2022.
- [2] S. A. Assefa, D. Dervovic, M. Mahfouz, R. E. Tillman, P. Reddy, and M. Veloso, “Generating synthetic data in finance: opportunities, challenges and pitfalls,” *Proceedings of the First ACM International Conference on AI in Finance*, pp. 1–8, 2020.
- [3] H. Ye, Z. Liu, X. Shen, W. Cao, S. Zheng, X. Gui, H. Zhang, Y. Chang, and J. Bian, “Uadb: Unsupervised anomaly detection booster,” in *2023 IEEE 39th International Conference on Data Engineering (ICDE)*. IEEE, 2023, pp. 2593–2606.
- [4] C. J. Urban and K. M. Gates, “Deep learning: A primer for psychologists,” *Psychological Methods*, vol. 26, no. 6, p. 743, 2021.
- [5] V. Borisov, T. Leemann, K. Seßler, J. Haug, M. Pawelczyk, and G. Kasneci, “Deep neural networks and tabular data: A survey,” *IEEE Transactions on Neural Networks and Learning Systems*, 2022.
- [6] X. Su, X. Yan, and C.-L. Tsai, “Linear regression,” *Wiley Interdisciplinary Reviews: Computational Statistics*, vol. 4, no. 3, pp. 275–294, 2012.
- [7] R. E. Wright, *Logistic regression*. American Psychological Association, 1995.
- [8] T. Chen and C. Guestrin, “Xgboost: A scalable tree boosting system,” *Proceedings of the 22nd acm sigkdd international conference on knowledge discovery and data mining*, pp. 785–794, 2016.
- [9] L. Prokhorenkova, G. Gusev, A. Vorobev, A. V. Dorogush, and A. Gulin, “Catboost: unbiased boosting with categorical features,” *Advances in neural information processing systems*, vol. 31, 2018.
- [10] K. He, X. Zhang, S. Ren, and J. Sun, “Deep residual learning for image recognition,” *Proceedings of the IEEE conference on computer vision and pattern recognition*, pp. 770–778, 2016.
- [11] I. Goodfellow, Y. Bengio, and A. Courville, *Deep Learning*. MIT Press, 2016, <http://www.deeplearningbook.org>.
- [12] J. Devlin, M.-W. Chang, K. Lee, and K. Toutanova, “Bert: Pre-training of deep bidirectional transformers for language understanding,” *arXiv preprint arXiv:1810.04805*, 2018.
- [13] Y. Gorishniy, I. Rubachev, V. Khruikov, and A. Babenko, “Revisiting deep learning models for tabular data,” *Advances in Neural Information Processing Systems*, vol. 34, pp. 18 932–18 943, 2021.
- [14] W. Song, C. Shi, Z. Xiao, Z. Duan, Y. Xu, M. Zhang, and J. Tang, “AutoInt: Automatic feature interaction learning via self-attentive neural networks,” *Proceedings of the 28th ACM international conference on information and knowledge management*, pp. 1161–1170, 2019.
- [15] A. Vaswani, N. Shazeer, N. Parmar, J. Uszkoreit, L. Jones, A. N. Gomez, E. Kaiser, and I. Polosukhin, “Attention is all you need,” *Advances in neural information processing systems*, vol. 30, 2017.

- [16] G. Klambauer, T. Unterthiner, A. Mayr, and S. Hochreiter, "Self-normalizing neural networks," *Advances in neural information processing systems*, vol. 30, 2017.
- [17] A. Kadra, M. Lindauer, F. Hutter, and J. Grabocka, "Well-tuned simple nets excel on tabular datasets," *Advances in neural information processing systems*, vol. 34, pp. 23 928–23 941, 2021.
- [18] H. Ye, W. Fan, X. Song, S. Zheng, H. Zhao, D. dan Guo, and Y. Chang, "PTaRL: Prototype-based tabular representation learning via space calibration," in *The Twelfth International Conference on Learning Representations*, 2024.
- [19] S. Ö. Arik and T. Pfister, "Tabnet: Attentive interpretable tabular learning," in *Proceedings of the AAAI conference on artificial intelligence*, vol. 35, no. 8, 2021, pp. 6679–6687.
- [20] J. Yoon, Y. Zhang, J. Jordan, and M. Van der Schaar, "Vime: Extending the success of self-and semi-supervised learning to tabular domain," *Advances in Neural Information Processing Systems*, vol. 33, pp. 11 033–11 043, 2020.
- [21] D. Bahri, H. Jiang, Y. Tay, and D. Metzler, "Scarf: Self-supervised contrastive learning using random feature corruption," in *International Conference on Learning Representations*, 2022.
- [22] T. Chen, S. Kornblith, M. Norouzi, and G. Hinton, "A simple framework for contrastive learning of visual representations," in *International conference on machine learning*. PMLR, 2020, pp. 1597–1607.
- [23] T. Ucar, E. Hajiramezani, and L. Edwards, "Subtab: Subsetting features of tabular data for self-supervised representation learning," *Advances in Neural Information Processing Systems*, vol. 34, pp. 18 853–18 865, 2021.
- [24] R. Wang, R. Shivanna, D. Cheng, S. Jain, D. Lin, L. Hong, and E. Chi, "Dcn v2: Improved deep & cross network and practical lessons for web-scale learning to rank systems," *Proceedings of the web conference 2021*, pp. 1785–1797, 2021.
- [25] A. Jeffares, T. Liu, J. Crabbé, F. Imrie, and M. van der Schaar, "Tangos: Regularizing tabular neural networks through gradient orthogonalization and specialization," in *The Eleventh International Conference on Learning Representations*, 2022.
- [26] G. Somepalli, A. Schwarzschild, M. Goldblum, C. B. Brass, and T. Goldstein, "SAINT: Improved neural networks for tabular data via row attention and contrastive pre-training," in *NeurIPS 2022 First Table Representation Workshop*, 2022. [Online]. Available: <https://openreview.net/forum?id=FiyUTAy4sB8>
- [27] I. Rubachev, A. Alekberov, Y. Gorishniy, and A. Babenko, "Revisiting pretraining objectives for tabular deep learning," *arXiv preprint arXiv:2207.03208*, 2022.
- [28] Z. Wang and J. Sun, "Transtab: Learning transferable tabular transformers across tables," *Advances in Neural Information Processing Systems*, vol. 35, pp. 2902–2915, 2022.
- [29] B. Zhu, X. Shi, N. Erickson, M. Li, G. Karypis, and M. Shoaran, "Xtab: Cross-table pretraining for tabular transformers," *arXiv preprint arXiv:2305.06090*, 2023.
- [30] C.-H. Chang, J. Yoon, S. Ö. Arik, M. Udell, and T. Pfister, "Data-efficient and interpretable tabular anomaly detection," in *Proceedings of the 29th ACM SIGKDD Conference on Knowledge Discovery and Data Mining*, 2023, pp. 190–201.
- [31] S. Oymak, Z. Fabian, M. Li, and M. Soltanolkotabi, "Generalization guarantees for neural networks via harnessing the low-rank structure of the jacobian," *arXiv preprint arXiv:1906.05392*, 2019.
- [32] X. Chen, S. Wang, M. Long, and J. Wang, "Transferability vs. discriminability: Batch spectral penalization for adversarial domain adaptation," in *International conference on machine learning*. PMLR, 2019, pp. 1081–1090.
- [33] Y. Xue, K. Whitecross, and B. Mirzasoleiman, "Investigating why contrastive learning benefits robustness against label noise," in *International Conference on Machine Learning*. PMLR, 2022, pp. 24 851–24 871.
- [34] H. Chen, J. Wang, A. Shah, R. Tao, H. Wei, X. Xie, M. Sugiyama, and B. Raj, "Understanding and mitigating the label noise in pre-training on downstream tasks," in *The Twelfth International Conference on Learning Representations*, 2024. [Online]. Available: <https://openreview.net/forum?id=TjhUtloBZU>
- [35] J. Nam, J. Tack, K. Lee, H. Lee, and J. Shin, "STUNT: Few-shot tabular learning with self-generated tasks from unlabeled tables," in *The Eleventh International Conference on Learning Representations*, 2023. [Online]. Available: https://openreview.net/forum?id=_xlsjehDvIY
- [36] D. D. V. M. Chary, "Prediction of full load electrical power output of a base load operated combined cycle power plant using machine learning methods," *SSRN Electronic Journal*, 2021. [Online]. Available: <https://api.semanticscholar.org/CorpusID:240033947>
- [37] K.-Y. Chen, P.-H. Chiang, H.-R. Chou, T.-W. Chen, and T.-H. Chang, "Trompt: Towards a better deep neural network for tabular data," in *International Conference on Machine Learning*. PMLR, 2023, pp. 4392–4434.
- [38] M. Cassotti, D. Ballabio, R. Todeschini, and V. Consonni, "A similarity-based qsar model for predicting acute toxicity towards the fathead minnow (pimephales promelas)," *SAR and QSAR in environmental research*, vol. 26 6, p. 521, 2015. [Online]. Available: <https://api.semanticscholar.org/CorpusID:11120429>
- [39] R. K. Pace and R. Barry, "Sparse spatial autoregressions," *Statistics & Probability Letters*, vol. 33, no. 3, pp. 291–297, 1997.
- [40] L. Grinsztajn, E. Oyallon, and G. Varoquaux, "Why do tree-based models still outperform deep learning on typical tabular data?" in *Neural Information Processing Systems*, 2022. [Online]. Available: <https://api.semanticscholar.org/CorpusID:252697222>
- [41] K. Hamidieh, "A data-driven statistical model for predicting the critical temperature of a superconductor," *Computational Materials Science*, 2018. [Online]. Available: <https://api.semanticscholar.org/CorpusID:55069173>
- [42] R. Kohavi *et al.*, "Scaling up the accuracy of naive-bayes classifiers: A decision-tree hybrid." *KDD*, vol. 96, pp. 202–207, 1996.
- [43] B. Schäfl, L. Gruber, A. Bitto-Nemling, and S. Hochreiter, "Hoplar: Modern hopfield networks for tabular data," in *NeurIPS 2023 Second Table Representation Learning Workshop*, 2023.
- [44] R. C. Madeo, C. A. Lima, and S. M. Peres, "Gesture unit segmentation using support vector machines: segmenting gestures from rest positions," in *Proceedings of the 28th Annual ACM Symposium on Applied Computing*, 2013, pp. 46–52.
- [45] T. Bertin-Mahieux, D. P. Ellis, B. Whitman, and P. Lamere, "The million song dataset," in *Proceedings of the 12th International Conference on Music Information Retrieval (ISMIR 2011)*, 2011.
- [46] J. A. Blackard and D. J. Dean, "Comparative accuracies of artificial neural networks and discriminant analysis in predicting forest cover types from cartographic variables," *Computers and electronics in agriculture*, vol. 24, no. 3, pp. 131–151, 1999.
- [47] H. Taud and J. Mas, "Multilayer perceptron (mlp)," *Geomatic approaches for modeling land change scenarios*, pp. 451–455, 2018.
- [48] G. Peyré, M. Cuturi *et al.*, "Computational optimal transport," *Center for Research in Economics and Statistics Working Papers*, pp. 2017–86, 2017.
- [49] R. F. Woolson, "Wilcoxon signed-rank test," *Wiley encyclopedia of clinical trials*, pp. 1–3, 2007.
- [50] S.-A. Liu, Y. Zhang, Z. Qiu, H. Xie, Y. Zhang, and T. Yao, "Learning orthogonal prototypes for generalized few-shot semantic segmentation," in *Proceedings of the IEEE/CVF Conference on Computer Vision and Pattern Recognition*, 2023, pp. 11 319–11 328.
- [51] Y. Jiang, B. Aragam, and V. Veitch, "Uncovering meanings of embeddings via partial orthogonality," *Advances in Neural Information Processing Systems*, vol. 36, 2024.
- [52] O. Roy and M. Vetterli, "The effective rank: A measure of effective dimensionality," in *2007 15th European signal processing conference*. IEEE, 2007, pp. 606–610.
- [53] V. Pappas, X. Han, and D. L. Donoho, "Prevalence of neural collapse during the terminal phase of deep learning training," *Proceedings of the National Academy of Sciences*, vol. 117, no. 40, pp. 24 652–24 663, 2020.
- [54] Y. Yang, S. Chen, X. Li, L. Xie, Z. Lin, and D. Tao, "Inducing neural collapse in imbalanced learning: Do we really need a learnable classifier at the end of deep neural network?" *Advances in neural information processing systems*, vol. 35, pp. 37 991–38 002, 2022.

APPENDIX

A. Nomenclature

For clarity, we summarize the key notations used throughout the paper in Table VIII. This includes the symbols, their definitions, and dimensionalities where applicable.

TABLE VIII: Notation.

Symbols	Description
x, y	Observed sample and the corresponding label.
N	Number of observed samples in a dataset.
$\mathcal{D}_{train}, \mathcal{D}_{val}, \mathcal{D}_{test}$	Training set, validation set, test set.
$F(\cdot; \theta)$	Deep tabular model.
$G_f(\cdot; \theta_f)$	Existing deep tabular backbone.
$G_h(\cdot; \theta_h)$	Prediction head.
z	Representation extracted by $G_f(\cdot; \theta_f)$.
D	Dimensionality of z .
\mathcal{L}	Loss function.
$\mathcal{Z} = \{z_i\}_{i=1}^N \in \mathbb{R}^{N \times D}$	Representations of N samples.
SVE	Singular Value Entropy.
\mathcal{Z}_o	Approximated optimal representations.
ϕ	Shift estimator.
$\tilde{\mathcal{Z}}_o$	Simulated sub-optimal representations derived from \mathcal{Z}_o .
Δ	$\tilde{\mathcal{Z}}_o$'s corresponding shift.
$\Phi(\cdot; \theta_\phi)$	Re-estimation function.
$T = \{\beta_t\}_{t=1}^T \in \mathbb{R}^{T \times D}$	Embedding vectors.
T	Number of embedding vectors.
β_t	t -th embedding vector.
LE-Space	Light Embedding Space consists of embedding vectors.
$s(\cdot; \theta_s)$	Coordinate estimator.
r	Coordinate of representation in the LE-Space.
$A \in [0, 1]^{T \times T}$	Cosine similarity between embedding vectors.

B. Ablation Study

We further conduct ablation study to demonstrate the effectiveness of key components of TRC. Specifically, we denote the task of tabular representation re-estimation as ‘‘TR’’, and for the task of tabular space mapping, we denote the process of space compression as ‘‘SC’’ and the strategy for diversifying the embedding vectors as ‘‘DE’’. Given that the strategy for diversifying the embedding vectors should be applied after the process of space compression, we conduct a comparative analysis between the backbone integrated with TRC and its five variants in Table IX.

C. Comparison with Deeper Backbone

Besides, TRC is appended to the output of the backbone $G_f(\cdot; \theta_f)$ while keeping the parameters fixed. We compare the performance of the backbone coupled with TRC against backbone with deeper layers (additional 3 layers) in Table X. Increasing the number of layers in backbone model does not necessarily lead to improved performance; in some cases, it even results in performance degradation. Furthermore, the comparison between deeper backbone and backbone augmented with TRC highlights that the well-designed tasks can significantly enhance model representations, which is not simply achieved by increasing model depth.

D. Training with Missing Value and Fewer Samples

TRC continues to enhance the performance of deep tabular models even under challenging conditions where training samples contain missing values and the overall number of training samples is reduced. We systematically increase the

TABLE IX: Analysis on the effects of different components of TRC. The best results are highlighted in bold, and the second best results are underscored. This table serves as an extension of Table III in manuscript.

	TR	SC	DE	CA ↓	CO ↓	DI ↓	QS ↓	SU ↓	PO ↓	AD ↑	AU ↑	GE ↑
MLP	✓			0.505	3.961	564.373	0.875	10.379	10.892	0.856	0.87	0.578
		✓		0.502	3.916	563.649	0.868	10.328	10.605	0.858	0.87	0.571
			✓	0.505	3.92	564.141	0.845	10.349	10.631	0.858	0.862	0.568
	✓	✓	✓	0.502	<u>3.908</u>	<u>558.52</u>	0.852	10.341	<u>10.602</u>	0.858	0.87	0.575
DCN2				0.495	4.016	591.958	1.027	10.674	8.805	0.856	0.841	0.564
	✓			0.493	3.912	579.461	0.941	10.521	8.795	0.858	0.848	0.575
		✓		0.498	4.016	580.454	<u>0.86</u>	10.634	8.757	0.858	0.848	0.565
			✓	0.495	3.844	<u>574.712</u>	0.884	10.727	8.782	0.858	0.841	0.563
SNN				0.496	4.023	580.247	0.853	10.634	8.764	0.858	0.855	0.567
	✓			0.493	<u>3.858</u>	574.453	0.879	<u>10.584</u>	8.79	0.857	0.862	0.584
		✓		0.896	11.789	1530.293	1.018	25.498	18.517	0.847	0.848	0.55
			✓	0.88	11.369	1226.754	0.921	25.265	15.86	0.847	0.855	0.572
ResNet				0.748	5.701	783.015	0.889	17.738	12.001	0.847	0.833	0.543
	✓			0.743	6.889	<u>696.473</u>	<u>0.886</u>	15.512	<u>11.422</u>	0.847	<u>0.862</u>	0.561
		✓		<u>0.742</u>	7.306	760.66	0.891	17.711	12.002	0.847	0.855	0.546
			✓	0.699	<u>6.88</u>	693.369	0.87	<u>15.537</u>	11.202	0.847	0.877	0.573
AutoInt				0.517	3.982	606.282	0.872	11.163	10.812	0.847	0.87	0.587
	✓			<u>0.512</u>	3.925	597.975	0.866	10.94	10.405	0.847	0.862	0.58
		✓		0.513	3.96	612.993	0.83	10.944	10.134	<u>0.849</u>	0.87	0.576
			✓	<u>0.512</u>	<u>3.922</u>	606.482	0.85	10.255	10.15	0.85	0.862	0.578
FT-Transformer				0.513	3.96	617.098	0.841	10.951	10.132	<u>0.849</u>	0.877	0.586
	✓			0.508	3.919	615.736	0.845	10.72	10.205	<u>0.849</u>	0.877	0.597
		✓		0.487	4.02	562.169	0.86	11.193	6.45	0.854	0.848	0.598
			✓	0.48	4.001	562.677	0.849	11.089	6.19	0.858	0.87	0.605
SAINT				0.48	4.001	559.535	0.835	10.86	5.694	0.857	0.855	0.591
	✓			0.477	3.971	555.787	0.828	10.972	5.88	0.856	0.891	0.59
		✓		0.48	4.003	559.341	0.842	<u>10.856</u>	5.685	0.856	0.87	0.595
			✓	0.477	3.96	<u>557.423</u>	<u>0.829</u>	10.826	5.885	0.858	0.891	0.606
VIME				0.469	3.709	551.19	0.823	10.41	2.919	0.858	0.848	0.611
	✓			0.463	3.685	549.075	0.819	10.295	2.71	0.861	<u>0.862</u>	0.61
		✓		0.464	3.668	549.684	0.812	10.338	2.759	0.861	0.855	0.62
			✓	0.462	<u>3.659</u>	543.504	0.806	<u>10.272</u>	2.76	0.862	<u>0.862</u>	<u>0.622</u>
SCARF				0.464	3.668	549.923	<u>0.797</u>	10.342	2.763	0.861	0.855	0.618
	✓			0.462	3.648	<u>543.653</u>	0.78	<u>10.223</u>	<u>2.728</u>	0.862	0.884	0.624
		✓		3.856	579.61	0.863	0.52	<u>7.292</u>	10.24	0.858	0.87	0.593
			✓	<u>3.839</u>	585.659	0.864	0.52	7.584	10.296	0.858	0.884	0.584
SAINT				3.841	588.05	0.829	0.521	7.485	10.233	0.858	0.877	0.586
	✓			3.827	571.684	0.837	0.52	7.212	10.292	0.855	0.884	0.587
		✓		3.841	572.493	0.835	0.523	7.325	10.201	0.859	0.87	0.584
			✓	3.847	577.803	0.808	0.52	7.531	10.355	0.859	0.884	0.589
VIME				0.508	4.022	597.207	0.827	13.095	4.415	0.857	0.87	0.549
	✓			0.491	3.911	559.944	0.822	12.868	4.403	0.857	0.862	0.579
		✓		0.495	3.869	565.402	0.81	12.813	4.358	0.857	0.87	0.581
			✓	0.492	3.911	556.744	0.823	12.85	4.329	0.856	0.884	0.586
VIME				0.495	3.869	565.393	0.821	<u>12.81</u>	4.365	0.857	0.87	0.584
	✓			0.491	3.903	<u>557.951</u>	0.818	12.443	<u>4.335</u>	0.858	0.884	0.595
		✓		0.679	5.218	945.238	1.018	15.645	10.914	0.768	0.812	0.473
			✓	<u>0.643</u>	4.378	707.749	0.952	15.486	7.365	0.847	0.87	0.473
VIME				0.645	4.174	<u>629.678</u>	0.96	15.537	6.861	0.846	0.87	0.472
	✓			0.645	<u>4.342</u>	638.677	0.957	<u>15.073</u>	7.443	0.847	0.877	0.472
		✓		0.648	4.378	644.659	0.949	15.544	7.799	0.846	0.877	0.476
			✓	0.645	4.371	612.454	<u>0.95</u>	15.028	7.489	0.846	0.884	0.479

TABLE X: Performance of backbone w/ TRC and deeper backbone. The depths of backbone layers are increased only for ‘‘deeper backbone’’. This table serves as an extension of Table IV in manuscript.

	CO ↓	DI ↓	QS ↓	CA ↓	PO ↓	SU ↓	AD ↑	AU ↑	GE ↑
MLP	3.961	564.373	0.875	0.505	10.892	10.379	0.856	0.870	0.578
deeper MLP	3.922	562.888	0.851	0.510	11.583	10.271	0.856	0.862	0.572
MLP+TRC	3.899	558.330	0.825	0.502	10.593	10.326	0.858	0.891	0.580
DCN2	4.016	591.958	1.027	0.495	8.805	10.674	0.856	0.841	0.564
deeper DCN2	3.872	575.765	0.904	0.486	9.165	10.675	0.858	0.862	0.575
DCN2+TRC	3.858	574.453	0.879	0.493	8.790	10.584	0.857	0.862	0.584
SNN	11.789	1530.293	1.018	0.896	18.517	25.498	0.847	0.848	0.550
deeper SNN	10.614	1042.509	1.121	0.851	14.460	15.039	0.847	0.833	0.553
SNN+TRC	6.880	693.369	0.870	0.699	11.202	15.537	0.847	0.877	0.573
ResNet	3.982	606.282	0.872	0.517	10.812	11.163	0.847	0.870	0.587
deeper ResNet	3.943	657.823	0.847	0.512	10.628	11.008	0.850	0.862	0.600
ResNet+TRC	3.919	615.736	0.845	0.508	10.205	10.720	0.849	0.877	0.597
AutoInt	4.020	562.169	0.860	0.487	6.450	11.193	0.854	0.848	0.598
deeper AutoInt	3.899	562.383	0.815	0.488	5.201	11.265	0.857	0.862	0.577
AutoInt+TRC	3.960	557.423	0.829	0.477	5.885	10.826	0.858	0.891	0.606
FT-Transformer	3.709	551.190	0.823	0.469	2.919	10.410	0.858	0.848	0.611
deeper FT-Transformer	3.604	559.363	0.786	0.464	2.850	10.142	0.860	0.870	0.623
FT-Transformer+TRC	3.648	543.653	0.780	0.462	2.728	10.223	0.862	0.884	0.624
SAINT	4.022	597.207	0.827	0.508	4.415	13.095	0.857	0.870	0.549
deeper SAINT	3.912	585.623	0.806	0.501	41.349	34.681	0.860	0.877	0.572
SAINT+TRC	3.903	557.951	0.818	0.491	4.335	12.443	0.858	0.884	0.595
VIME	5.218	945.238	1.018	0.679	10.914	15.645	0.768	0.812	0.473
deeper VIME	4.348	690.491	0.969	0.651	5.984	15.332	0.843	0.877</	

performance. Nevertheless, by leveraging TRC, we are able to consistently enhance the capabilities of the deep tabular model, thereby alleviating the negative impact of data incompleteness and scarcity.

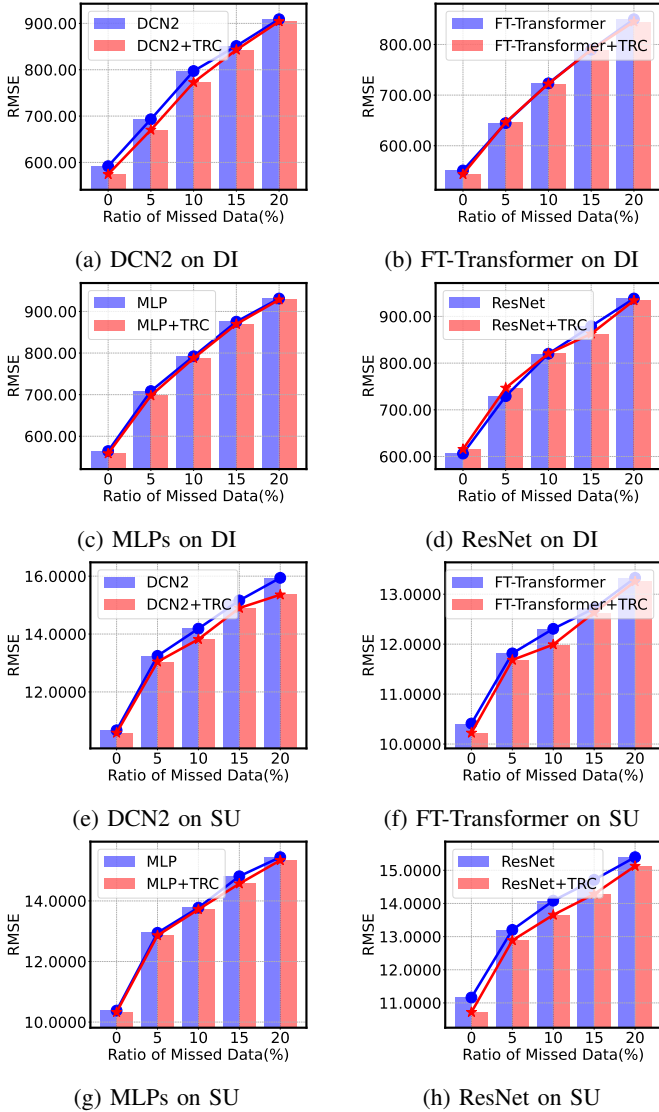


Fig. 12: The results of TRC training with missing values. This figure serves as an extension of Fig. 7 in manuscript.

E. Parameter Analysis

The proposed TRC provides a parameter-efficient, cost-effective technique to enhance the representations of deep tabular backbones without altering any of their parameters. As shown in Fig. 14, the parameter quantity of TRC is significantly lower compared to deep tabular models, particularly for the FT-Transformer model, which inherently has a large number of parameters.

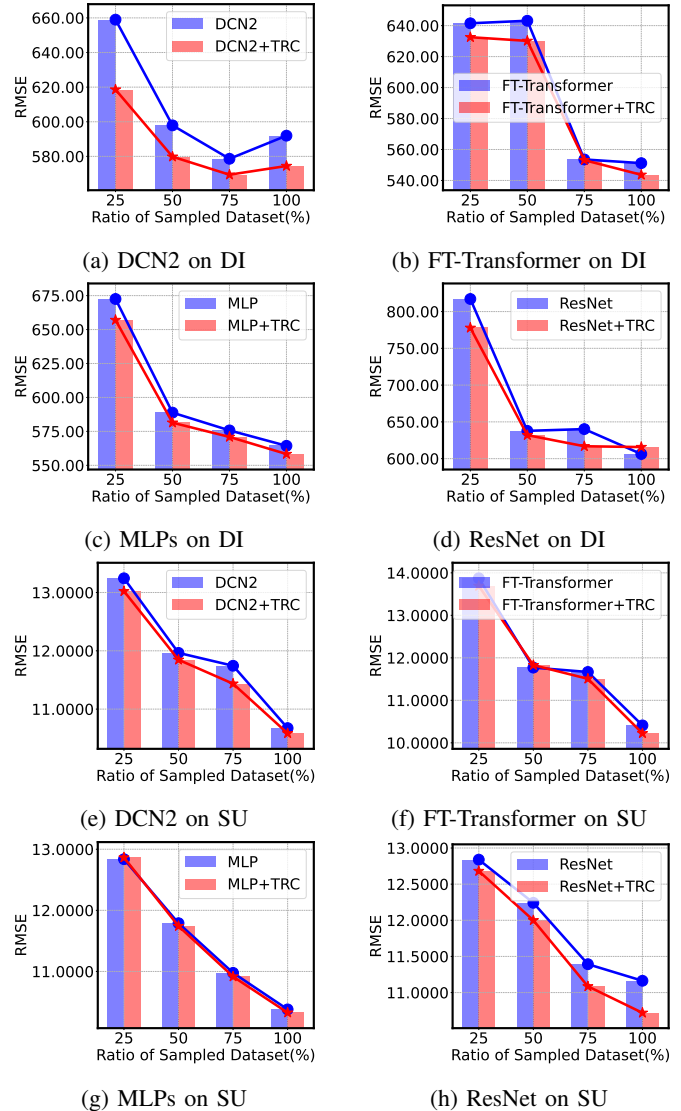


Fig. 13: The results of TRC training with fewer samples. This figure serves as an extension of Fig. 7 in manuscript.

F. Computational Efficiency

We provide training and inference time cost in Table XI and Table XII. All experiments were conducted on the Ubuntu 20.04.4 LTS operating system, Intel(R) Xeon(R) Gold 5220 CPU @ 2.20GHz with single NVIDIA A40 48GB GPU and 512GB of RAM. Since TRC does not need to retrain the deep tabular backbone, the training time of TRC is noticeably reduced compared to the deep tabular model in most cases. In addition, the inference cost of TRC is also much smaller compared to deep tabular backbones, thus will not introduce high inference overhead to the existing backbones. The relatively higher inference time for both backbone and TRC observed on the YE and COV datasets are primarily due to their large sizes, as shown in Table I of manuscript.

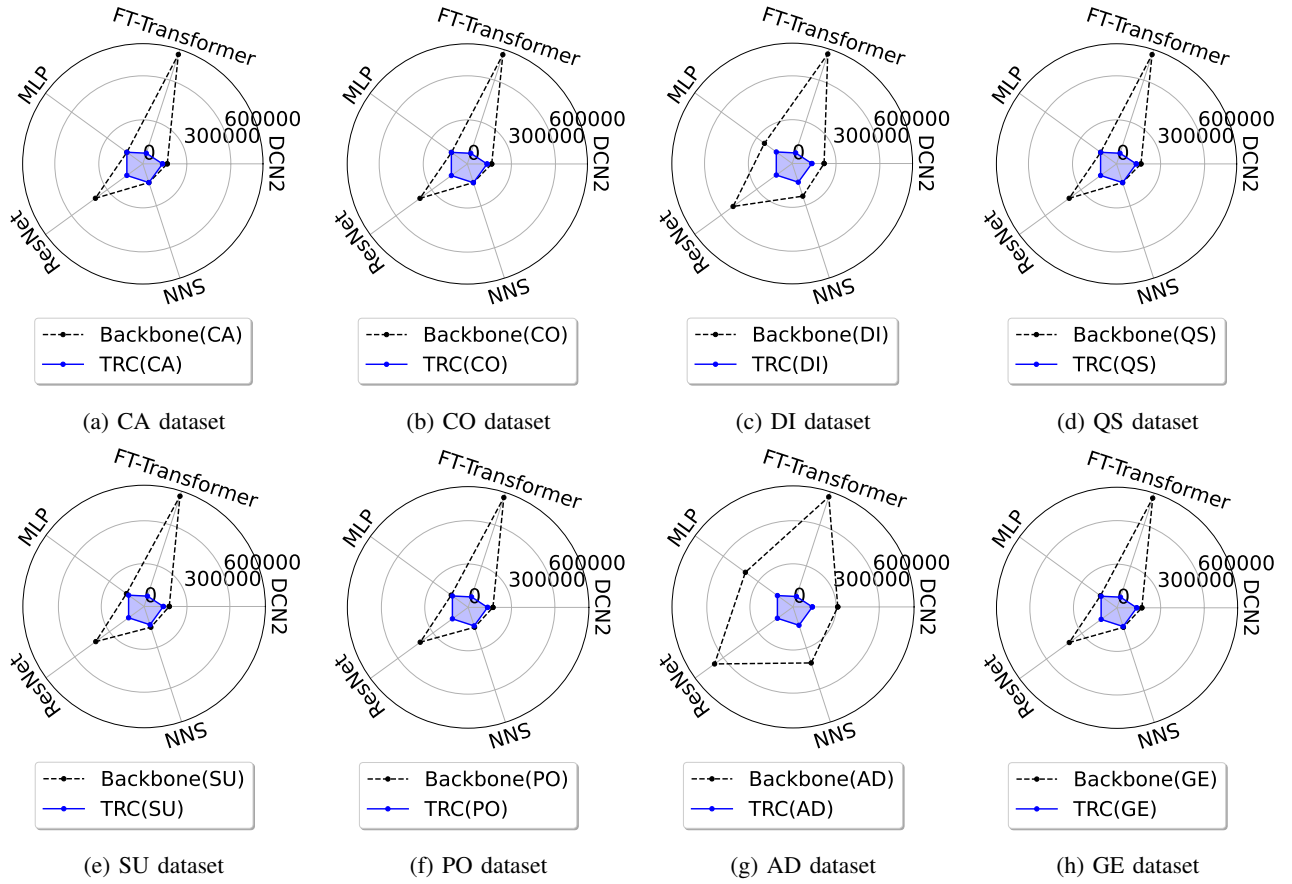


Fig. 14: The comparison of parameters between TRC and deep tabular models. This figure serves as an extension of Fig. 9 in manuscript.

TABLE XI: Time cost (seconds) per training epoch on the full training set. The training time for TRC does not include the training cost for backbone model.

	CO	DI	QS	CA	PO	SU	AD	AU	GE	YE	COV
MLP	0.129	0.719	0.013	0.267	0.189	0.285	0.566	0.011	0.123	9.259	9.442
TRC	0.171	0.878	0.020	0.348	0.248	0.372	0.688	0.017	0.167	13.086	13.818
ResNet	0.188	1.092	0.020	0.399	0.282	0.424	0.864	0.016	0.184	15.285	13.948
TRC	0.168	0.880	0.021	0.354	0.249	0.374	0.698	0.018	0.167	13.629	12.909
FT-Transformer	0.424	2.348	0.045	0.917	0.685	1.397	1.857	0.038	0.431	68.678	52.186
TRC	0.174	0.891	0.027	0.356	0.259	0.382	0.705	0.024	0.174	13.200	13.194
SCARF	8.972	3.368	0.043	1.435	0.873	1.331	2.485	0.034	0.593	22.253	22.083
TRC	4.882	1.145	0.032	0.452	0.317	0.474	0.908	0.027	0.216	12.974	13.113
VIME	0.619	2.974	0.272	1.061	1.197	2.169	2.972	0.261	0.776	43.997	36.498
TRC	0.270	1.332	0.037	0.512	0.398	0.582	1.099	0.028	0.260	11.700	13.356

TABLE XII: Inference time cost (seconds) on the full test set. The inference time for TRC does not include the inference time for backbone model.

	CO	DI	QS	CA	PO	SU	AD	AU	GE	YE	COV
MLP	0.007	0.053	0.003	0.015	0.012	0.013	0.081	0.003	0.009	0.177	0.397
TRC	0.006	0.032	0.002	0.013	0.011	0.011	0.053	0.002	0.006	0.151	0.297
ResNet	0.016	0.111	0.006	0.042	0.030	0.034	0.147	0.006	0.020	0.433	0.970
TRC	0.005	0.033	0.002	0.015	0.010	0.012	0.043	0.002	0.006	0.154	0.341
FT-Transformer	0.042	0.275	0.012	0.130	0.131	0.180	0.512	0.012	0.083	2.704	4.600
TRC	0.005	0.030	0.001	0.014	0.010	0.012	0.051	0.001	0.007	0.142	0.318
Scarf	0.007	0.051	0.003	0.016	0.012	0.014	0.080	0.003	0.009	0.175	0.413
TRC	0.006	0.034	0.002	0.014	0.009	0.012	0.047	0.002	0.007	0.137	0.337
VIME	0.008	0.073	0.004	0.019	0.015	0.015	0.149	0.004	0.011	0.222	0.480
TRC	0.005	0.030	0.002	0.013	0.010	0.010	0.046	0.002	0.006	0.138	0.268

G. Visualization

We provide the TSNE visualization of coefficients for embedding vectors in Fig. 15, the visualization of the similarity matrix for embedding vectors in Fig. 16, and the heatmap of coefficients for embedding vectors in Fig. 17.

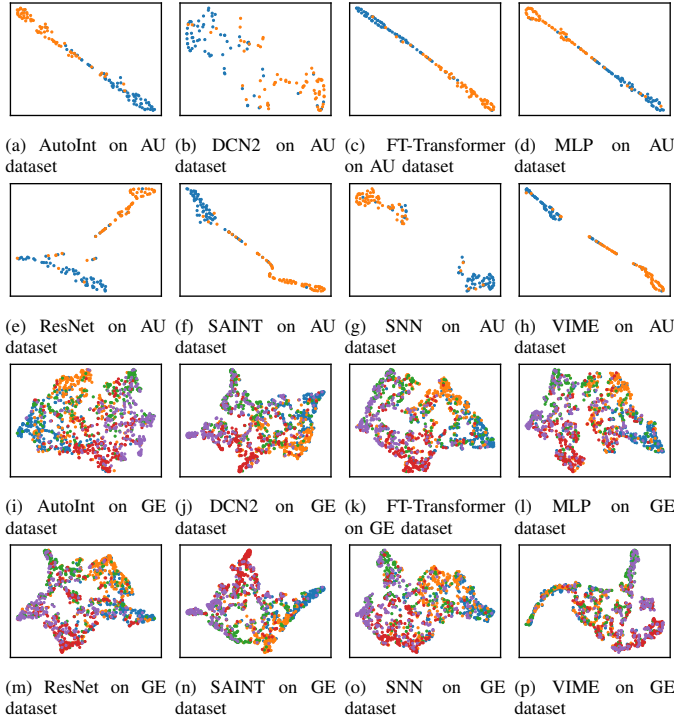


Fig. 15: The TSNE visualization of coefficients for embedding vectors.

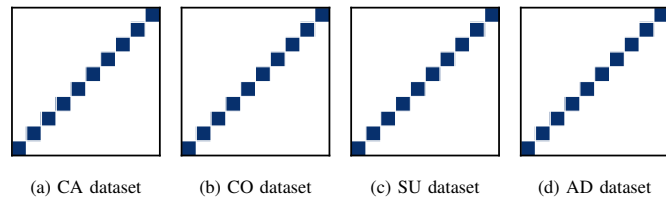


Fig. 16: The visualization of the similarity matrix for embedding vectors on FT-Transformer.

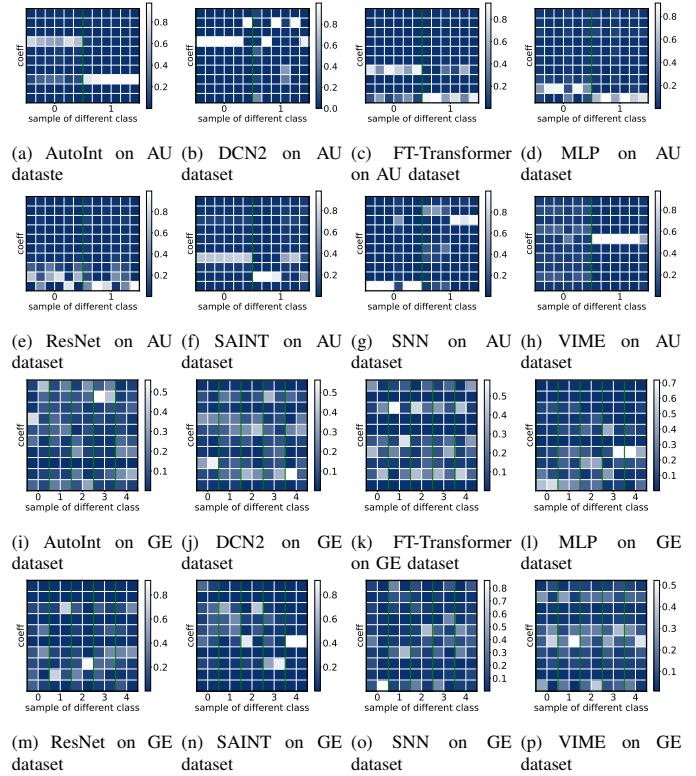


Fig. 17: The visualization of coefficients for embedding vectors.

H. The Relationship between SVE and the Number of Embedding Vectors

We provide the relationship between SVE and the number of embedding vectors in Fig. 18.

I. Sensitivity Analysis

We incorporate the sensitivity analysis for the weight of loss function \mathcal{L}_{orth} , the perturbing times for constructing simulated sub-optimal representations in Inherent Shift Learning, the ratio of selected optimal representations, and the number of embedding vectors in Fig. 19, Fig. 20, Fig. 21, and Fig. 22.

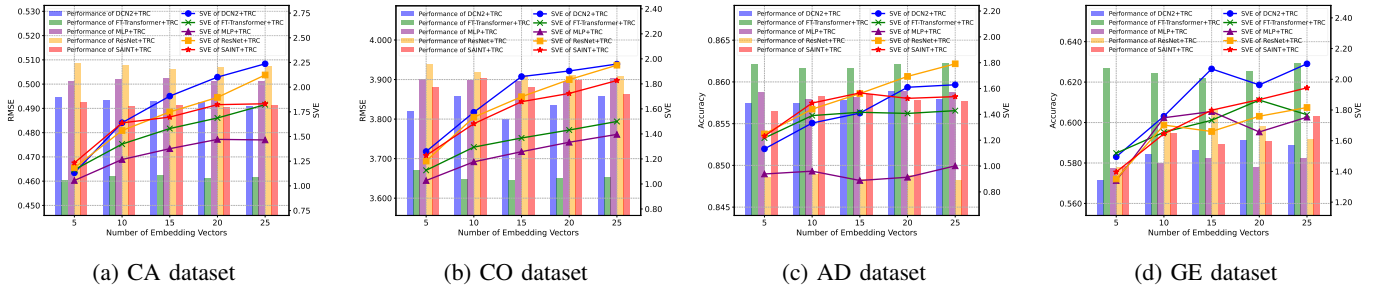


Fig. 18: Increasing the number of embedding vectors leads to larger SVE values of representations.

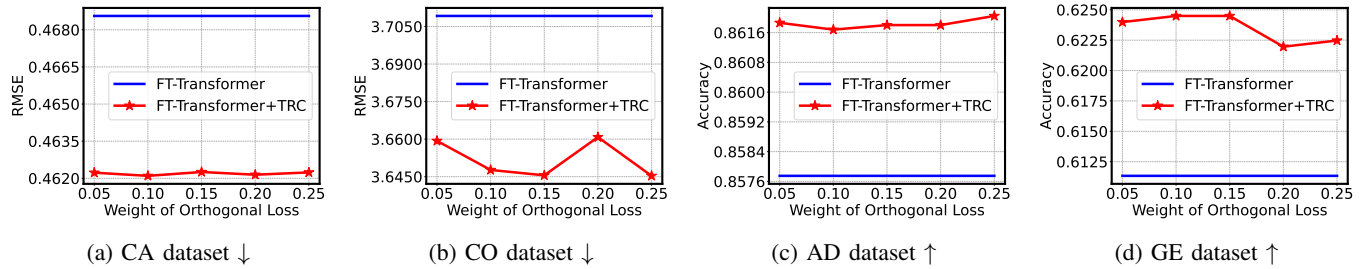


Fig. 19: The performance of TRC with varying weights of the orthogonality loss.

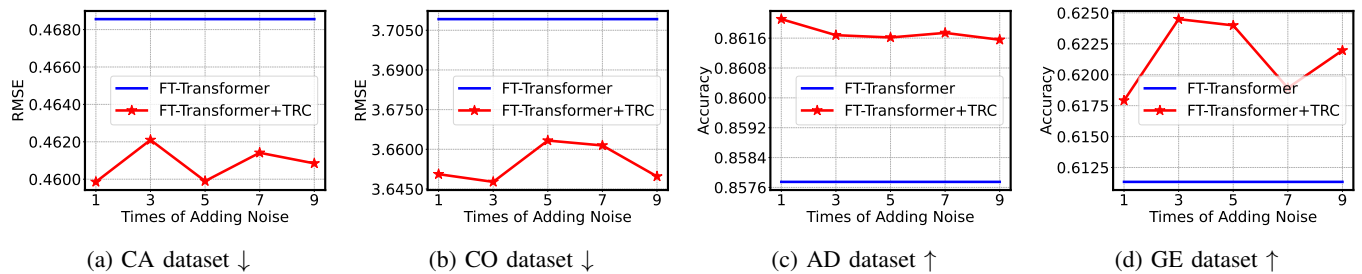
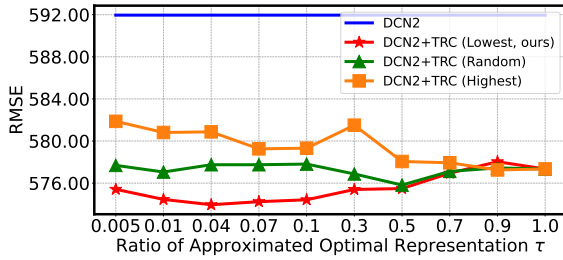
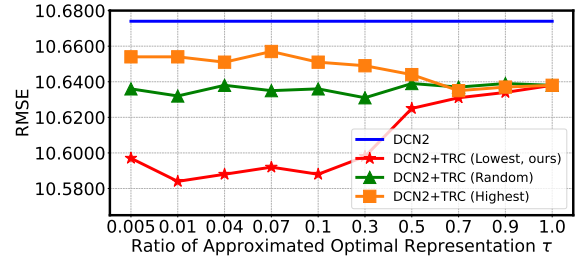


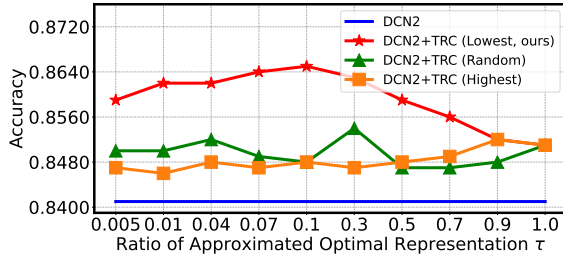
Fig. 20: The performance of TRC with varying times of perturbing the observation in Inherent Shift Learning.



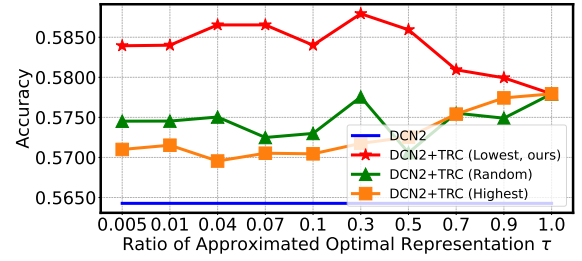
(a) DI dataset ↓



(b) SU dataset ↓

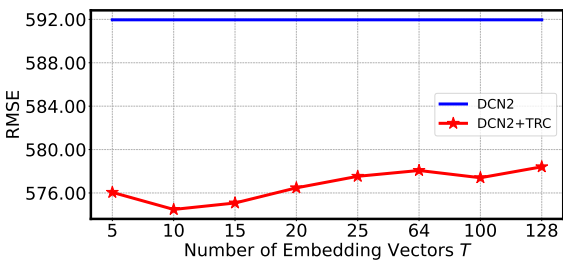


(c) AU dataset ↑

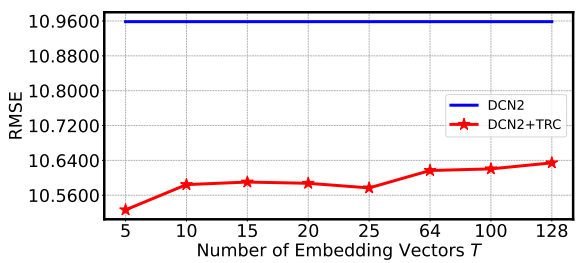


(d) GE dataset ↑

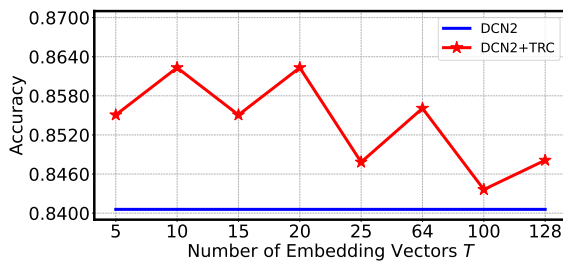
Fig. 21: The performance of TRC with the varying proportion of the selected optimal representation over all of the validation set samples, i.e., τ . This figure serves as an extension of Fig. 10 in manuscript.



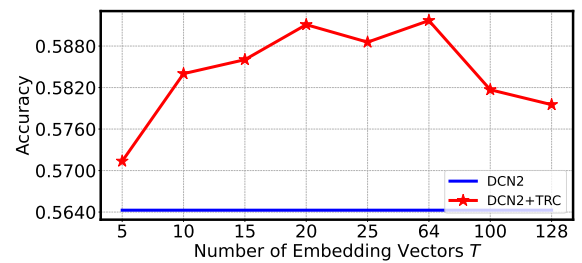
(a) DI dataset ↓



(b) SU dataset ↓



(c) AU dataset ↑



(d) GE dataset ↑

Fig. 22: The performance of TRC with varying number of embedding vectors. This figure serves as an extension of Fig. 11 in manuscript.

J. Theoretical Analysis and Discussion

Definition 3 Effective Rank. *The effective rank [52] of the matrix \mathcal{Z} , denoted $\text{erank}(\mathcal{Z})$, is defined as:*

$$\text{erank}(\mathcal{Z}) = \exp(\text{SVE}), \quad (13)$$

where SVE is the entropy of normalized singular values, as defined in **Definition 1**. The effective rank can be considered as a real-valued extension of the rank. While the usual rank counts the number of non-zero singular values, the effective rank measures how the energy is distributed across the singular directions.

To intuitively understand the difference between rank and effective rank, consider a two-dimensional Gaussian random vector with highly correlated components. Its covariance matrix is of rank two, but the corresponding Gaussian distribution exhibits most of its energy along the direction of one singular vector. In such a case, the spectral entropy (SVE) approaches zero, where the effective rank is slightly greater than one.

Lemma 1 *Let $\mathcal{Z} = \{z_i\}_{i=1}^N \in \mathbb{R}^{N \times D}$ denote the representations, where N is the number of samples and D is the dimensionality. Then we have*

$$\text{SVE}(\mathcal{Z}) = \log \text{erank}(\mathcal{Z}) \leq \log \text{rank}(\mathcal{Z}), \quad (14)$$

which is given by [52].

Proposition 1 *Consider a classification task with C classes. Let $\mathcal{Z} = \{z_i\}_{i=1}^N \in \mathbb{R}^{N \times D}$ and $Y \in \mathbb{R}^{N \times C}$ denote the representations and one-hot label matrix, where N is the number of samples, D is the dimensionality and $C \leq D$. When the model is trained to near-zero loss, the SVE of \mathcal{Z} satisfies $\text{SVE}(\mathcal{Z}) \leq \log C$.*

Proof. Assuming a balanced dataset, when the model is trained to near-zero loss, the phenomenon neural collapse typically occurs [53], [54]. This implies that all representations within a class converge to their within-class means. Specifically, for class c , all representations $\{z_i\}$ belongs to class c satisfies $z_i \rightarrow w_c$, where $w_c \in \mathbb{R}^D$ is the class center. Thus representation \mathcal{Z} could be written as

$$\mathcal{Z} = YW, \quad (15)$$

where $W = \{w_c\}_{c=1}^C \in \mathbb{R}^{C \times D}$ contains the class centers as rows. From properties of matrix multiplication, the rank of \mathcal{Z} is upper bounded by:

$$\text{rank}(\mathcal{Z}) \leq \min(\text{rank}(Y), \text{rank}(W)) \leq \min(C, D) = C. \quad (16)$$

Then we have:

$$\text{SVE}(\mathcal{Z}) \leq \log \text{rank}(\mathcal{Z}) \leq \log C, \quad (17)$$

which is given by **Lemma 1**.

Discussion 1: SVE interpretation in TRC. TRC focuses on deep learning for supervised tabular prediction tasks, i.e., classification and regression. The purpose is to model the conditional distribution $P(y|x)$, where x and y are features and corresponding label. As we discussed in Section III of manuscript, the typical architecture used for such tasks consists of a backbone network that extracts latent representations, followed by a linear prediction head. Let us take classification as an example to illustrate. Ideally, the learned representations

should be linearly separable: that is, representations for the same class should cluster together, and different classes should be well-separated.

Let $\mathcal{Z} = \{z_i\}_{i=1}^N \in \mathbb{R}^{N \times D}$ denote the representations, where N is the number of samples, D is the dimensionality and $D \leq N$. As shown in **Lemma 1** in Appendix J, we have $\text{SVE}(\mathcal{Z}) \leq \log \text{Rank}(\mathcal{Z}) \leq \log D$, where SVE denotes singular value entropy. **Proposition 1** in Appendix J establishes that for well-learned representations that are informative for the prediction task, the energy tends to concentrate in a few dominant singular directions. As a result, the SVE is upper bounded by $\log C$, where C is the number of classes and $C \leq D$. We assume that the trained deep tabular backbones has learned redundant information in addition to useful information for prediction. This is supported by our empirical results in Fig. 2 and Fig. 6 of manuscript, where higher SVE often exhibits worse performance. In addition, we could observe from Fig. 8 of manuscript that with the redundant information (higher SVE), the representations tend to be more entangled and less linearly separable.

Our method, TRC, leverages this insight to improve learned representations in a post-hoc, model-agnostic fashion. It reduces SVE while maintaining predictive performance, by jointly minimizing the supervised loss (Eq. 12) and the entropy of the singular value spectrum. This avoids modifying the original backbone and retains its capacity to learn complex feature interactions. Importantly, we do not advocate for extreme compression: excessively low SVE can discard task-relevant information and cause underfitting. Our results show that moderate SVE reduction strikes a good balance between compactness and predictive utility (Fig. 6 and Fig. 8 of manuscript).

Proposition 2 *Let $\mathcal{Z}^* \in \mathbb{R}^{N \times D}$ denote the representations obtained by Tabular Space Mapping in TRC, where N is the number of samples, D is the dimensionality and T is the number of embedding vectors with $T \leq D$. Then we have $\text{SVE}(\mathcal{Z}^*) \leq \log T$.*

Proof. Given that any representation computed by Eq. 9 in Tabular Space Mapping of manuscript could be viewed as a weighted linear combination of the embedding vectors $r\mathcal{B}$, \mathcal{Z}^* could be written as:

$$\mathcal{Z}^* = R\mathcal{B}, \quad (18)$$

where $R = \{r_i\}_{i=1}^N \in \mathbb{R}^{N \times T}$ denotes the weights across all samples, and $\mathcal{B} \in \mathbb{R}^{T \times D}$ denotes the embedding vectors. From properties of matrix multiplication, the rank of \mathcal{Z}^* is upper bounded by:

$$\text{rank}(\mathcal{Z}^*) \leq \min(\text{rank}(R), \text{rank}(\mathcal{B})) \leq \min(T, T) = T. \quad (19)$$

Then we have:

$$\text{SVE}(\mathcal{Z}^*) \leq \log \text{rank}(\mathcal{Z}^*) \leq \log T, \quad (20)$$

which is given by **Lemma 1**.

Discussion 2: The choice of number of embedding vectors T in TRC. Let $\mathcal{Z} = \{z_i\}_{i=1}^N \in \mathbb{R}^{N \times D}$ and $\mathcal{Z}^* \in \mathbb{R}^{N \times D}$ denote the representations obtained by backbone and Tabular Space Mapping in TRC respectively, where N is the number of samples and D is the dimensionality. As

discussed in **Discussion 1**, the deep tabular backbones often exhibits high SVE, indicating that the learned representations \mathcal{Z} contain redundancy in addition to task-relevant information. We propose to jointly reduce the SVE of \mathcal{Z}^* and minimize the supervised loss in Eq. 12 of manuscript to remain the critical information for prediction. This encourages the energy of representations to concentrate along dominant singular directions that are most informative for the task.

As illustrated in **Proposition 2**, SVE of \mathcal{Z}^* is upper bounded by $\log T$, where T is the number of embedding vectors in LE-Space. Therefore the reduction of SVE could be achieved by decreasing the number of embedding vectors T . To make the SVE of \mathcal{Z}^* in TRC effectively less than that of \mathcal{Z} from backbone models, one could calculate the SVE of \mathcal{Z} on train set, and set $T < \exp(\text{SVE}(\mathcal{Z}))$. Notably, overly low SVE values may lead to underfitting by discarding useful task-relevant information. Hence, we recommend choosing T in a moderate range (e.g., $[5, \exp(\text{SVE}(\mathcal{Z}))]$) to maintain a good balance between compression and information preservation.

The sensitivity analysis w.r.t. T are presented in Fig. 11 of manuscript and Fig. 22 of Appendix I. Overall, the TRC is robust across a wide range of T , and TRC consistently improve the performance of backbone models across all values of T . As we suggested, when T is within the range of $[5, \exp(\text{SVE}(\mathcal{Z}))]$ (e.g., $\exp(\text{SVE}(\mathcal{Z})) = 22$ on CO dataset, $\exp(\text{SVE}(\mathcal{Z})) = 29$ on DI dataset, $\exp(\text{SVE}(\mathcal{Z})) = 94$ on SU dataset, $\exp(\text{SVE}(\mathcal{Z})) = 81$ on AU dataset, $\exp(\text{SVE}(\mathcal{Z})) = 101$ on GE dataset), the performance of TRC is stable. As T increases further, we observe a slight degradation in performance, yet TRC could still enhance the performance of backbone model. This is aligned with our claim that higher SVE may introduce redundant information hindering prediction.

K. How Well the Simulated Shift is Expected to Model the “Inherent” Shift

We include experiment to evaluate how well the simulated shift, computed by shift estimator, can model the real inherent shift. The results are provided in Table XIII. Let us denote the representations extracted by the trained backbone $G_f(\cdot; \theta_f)$ as $\mathcal{Z} = \{z_i\}_{i=1}^N \in \mathbb{R}^{N \times D}$, where $z_i = G_f(x_i; \theta_f) \in \mathbb{R}^D$ corresponds to sample x_i , N is the number of samples. The true inherent shift is defined by the discrepancy between sub-optimal representation and the corresponding optimal representation. However, since the true optimal representations are not accessible in practice, directly measuring the inherent shift is challenging.

To approximate this, we propose the following experimental setup: we train the same backbone architecture $G_f(\cdot; \theta_f)$ in two different ways, (i) heavy training with the full number of epochs, producing representations $\mathcal{Z}^{\text{heavy}} = \{z_i^{\text{heavy}}\}_{i=1}^N$, and (ii) light training with only half the number of epochs, yielding $\mathcal{Z}^{\text{light}} = \{z_i^{\text{light}}\}_{i=1}^N$. We make an assumption that compared to the representations $\mathcal{Z}^{\text{light}}$ from light training, the representations $\mathcal{Z}^{\text{heavy}}$ from heavy training are closer to the optimal ones. Hence, we treat $\mathcal{Z}^{\text{heavy}}$ as optimal representations, and $\mathcal{Z}^{\text{light}}$ as sub-optimal representations. Notably, this assumption is adopted solely for the purpose of this evaluation, in the absence of ground truth for the inherent shift.

TABLE XIII: The L2 distance between sub-optimal representations and optimal representations w/o and w/ shift estimator. “w/o Shift Estimator” corresponds to the distance between z_i^{light} and z_i^{heavy} , “w/ Shift Estimator” corresponds to the distance between \hat{z}_i and z_i^{heavy} .

Backbone	Discrepancy (\downarrow)	AD	CA	CO	GE
MLP	w/o Shift Estimator	0.647	0.487	0.450	0.464
MLP	w/ Shift Estimator	0.578	0.395	0.246	0.434
FT-Transformer	w/o Shift Estimator	2.217	2.460	2.352	3.870
FT-Transformer	w/ Shift Estimator	1.068	0.887	0.820	1.443

Under this setup, the true inherent shift for each z_i^{light} is defined as $z_i^{\text{light}} - z_i^{\text{heavy}}$. We apply the proposed TRC to $\mathcal{Z}^{\text{light}}$ and obtain the learned shift estimator $\phi(\cdot; \theta_\phi)$. Next, we apply our shift estimator $\phi(\cdot; \theta_\phi)$ to estimate the inherent shift on each z_i^{light} , and obtain the re-estimated representation \hat{z}_i by $\hat{z}_i = z_i^{\text{light}} - \phi(z_i^{\text{light}}; \theta_\phi)$. Intuitively, if the estimated shift $\phi(\cdot; \theta_\phi)$ could well model the true inherent shift $z_i^{\text{light}} - z_i^{\text{heavy}}$, \hat{z}_i should be closer to z_i^{heavy} . We then compare the average distance between \hat{z}_i and z_i^{heavy} , against the average distance between z_i^{light} and z_i^{heavy} .

Our results show that the re-estimated representation \hat{z}_i are significantly closer to the optimal representation z_i^{heavy} than the original suboptimal ones z_i^{light} . This demonstrates that the shift estimator learned from artificial corruption has the potential ability to model the inherent shift in the representation space.

L. Limitations of Assumption 1

We acknowledge that the assumption may not always hold. In particular, as shown in Table XIV, when the backbone model is severely underfitting and far from convergence (e.g., trained for only 5% of the total epochs), the performance of TRC based on Assumption 1 (lowest-gradient selection) becomes similar to that of random or highest-gradient selection. This suggests that, under severe backbone underfitting settings, low gradient norms may not indicate representations with the least shift. However, when the number of training epochs increases, e.g., trained for 50% of the total epochs, TRC based on Assumption 1 could enhance the backbone performance better than that of random or highest-gradient selection, which illustrates the effectiveness of Assumption 1.

M. Broader Impacts

Tabular data is extensively utilized across various domains including healthcare, finance, engineering and psychology. Despite its wide-ranging application, much of the research in deep learning, has predominantly focused on other data modalities such as images, text, and time series. Our paper aims to bridge this gap by introducing a novel deep Tabular Representation Corrector, TRC, to enhance trained deep tabular models through two tasks. Progress in this direction has the potential to facilitate the construction of multi-modal pipelines for problems where only one part of the input is tabular, while other components involve images, text, and other

TABLE XIV: The performance of TRC on underfitted backbone.

Datasets	Backbone training epochs	DCN2	+TRC (Lowest, ours)	+TRC (Random)	+TRC (Highest)
CO ↓	5%	4.57	4.498	4.512	4.503
CO ↓	50%	4.384	4.165	4.285	4.325
GE ↑	5%	0.508	0.527	0.525	0.524
GE ↑	50%	0.543	0.561	0.55	0.548

Deep Learning-friendly data types. These pipelines can then be trained end-to-end through gradient optimization across all modalities. Such integration enables the fusion of insights from tabular data, such as demographics and genomics, with information from images, text, and time series.